MNRAS 000, 1–?? (2016) Preprint 11 January 2019 Compiled using MNRAS LATEX style file v3.0

A machine learning approach for identification and classification of symbiotic stars using 2MASS and WISE

Stavros Akras[1,2]★,†, Marcelo L. Leal-Ferreira[3,4]‡, Lizette Guzman-Ramirez[3,5], Gerardo Ramos-Larios[6]

[1] *Observatório Nacional/MCTI, Rua Gen. José Cristino, 77, 20921-400, Rio de Janeiro, Brazil*
[2] *Observatório do Valongo, Universidade Federal do Rio de Janeiro, Ladeira Pedro Antonio 43, 20080-090, Rio de Janeiro, Brazil*
[3] *Leiden Observatory, Leiden University, Niels Bohrweg 2, 2333 CA Leiden, Netherlands*
[4] *Argelander-Institut für Astronomie, Universitüt Bonn, Auf dem Hügel 71, 53121, Bonn, Germany*
[5] *European Southern Observatory, Alonso de Córdova 3107, Casilla 19001, Santiago, Chile*
[6] *Instituto de Astronomía y Meteorología, Av. Vallarta No. 2602, Col. Arcos Vallarta, C.P. 44130 Guadalajara, Jalisco, Mexico*

Accepted XXX. Received YYY; in original form ZZZ

ABSTRACT

In this second paper in a series of papers based on the most-up-to-date catalogue of symbiotic stars (SySts), we present a new approach for identifying and distinguishing SySts from other Hα emitters in photometric surveys using machine learning algorithms such as classification tree, linear discriminant analysis, and K-nearest neighbour. The motivation behind of this work is to seek for possible colour indices in the regime of near- and mid-infrared covered by the 2MASS and WISE surveys. A number of diagnostic colour-colour diagrams are generated for all the known Galactic SySts and several classes of stellar objects that mimic SySts such as planetary nebulae, post-AGB, Mira, single K and M giants, cataclysmic variables, Be, AeBe, YSO, weak and classical T Tauri stars, and Wolf-Rayet. The classification tree algorithm unveils that primarily *J–H*, *W1–W4* and K_s–*W3* and secondarily *H–W2*, *W1–W2* and *W3–W4* are ideal colour indices to identify SySts. Linear discriminant analysis method is also applied to determine the linear combination of 2MASS and AllWISE magnitudes that better distinguish SySts. The probability of a source being a SySt is determined using the K-nearest neighbour method on the LDA components. By applying our classification tree model to the list of candidate SySts (Paper I), the IPHAS list of candidate SySts, and the DR2 VPHAS+ catalogue, we find 125 (72 new candidates) sources that pass our criteria while we also recover 90 per cent of the known Galactic SySts.

Key words: general: catalogues - stars: binaries: symbiotic - stars: fundamental parameters - methods: statistical - methods: data analysis

1 INTRODUCTION

This is the second in a series of papers based on the new catalogue of symbiotic stars (SySts). In Paper I (Akras et al. 2019, accepted for publication in ApJS) the compilation of known (323) and candidate (87) SySts as well as an atlas of 348 spectral energy distributions (SED) from 1 to 22μm, using the Two Micron All Sky Survey (2MASS, Skrutskie et al. 2006) and the Wide-field Infrared Survey Explorer (WISE, Wright et al. 2010) data are presented. The classification of all known SySts in the S-D-D′scheme, based on their SED profiles, is revised. Seventy-four per cent are classified as S-type (stellar), 13 per cent as D-type (dusty), 8 per cent as S+IR-type (stellar + infrared excess) and 3.5 per cent as D′-type.

SySts are ideal astrophysical laboratories for investigating and studying the formation of aspherical circumstellar envelopes, mass transfer accretion disks processes, formation of soft and hard-X rays emission, dust forming regions, colliding winds among others (e.g. Jordan et al. 1996; Totov 2003; Sokoloski 2003; Leedjärv 2004, Mikolajewska 2012; Luna et al. 2013, Skopal & Carikovía 2015; Mukai et al.

★ CNPq Fellow (PDI-DA 300336/2016-0)
† e-mail: stavrosakras@on.br
‡ CNPq Fellow (248503/2013-8)

2016). Beside all these phenomena and processes, they are also considered as candidates for the progenitors of type Ia supernova (SN Ia, Munari & Renzini 1992; Han & Podsiadlowski 2004; Di Stefano 2010; Wang et al. 2010; Dilday et al. 2012).

Yet, the numbers of known SySts in the Milky Way (257, Paper I) and nearby galaxies (66, Paper I) are still far from being consistent with the expected number derived from population models (e.g. $3{\times}10^5$, Munari & Renzini 1992; $4{\times}10^5$, Magrini, Corradi & Munari 2003; 1.2-$15{\times}10^3$, Lü, Yungelson & Han 2016).

Many attempts have been made to discover new members by developing diagnostic colour-colour diagrams (DCCD) in the optical ([O III] 4363/H γ vs. [O III] 5007/H β, Gutierrez-Moreno, Moreno & Cortés 1995; various combinations of emission line ratios, Ilkiewicz & Mikolajewska 2017; r–H α vs. r–i, Corradi et al. 2008, 2010; Rodríguez-Flores et al. 2014), near-IR (J–H vs. H–K_s, Allen & Glass 1974; Phillips 2007; Corradi et al. 2008; Clyne et al. 2015, I–J vs. J–K_s, Schmeja & Kimeswenger 2001) and mid-IR regime (K-[12] vs. [12]-[25], Luud & Tuvikene 1987; Leedjärv 1992).

The motivation of this work is to find new colour criteria in the regime of near and mid-IR that will identify SySts using machine learning algorithms. Recall that SySts display SED peaks in the wavelength range between ~1 and ~25μm (Ivison et al. 1995, Paper I). Therefore, the 2MASS/WISE surveys are very helpful to distinguish SySts from other strong H α emitters (e.g. genuine planetary nebulae (PNe), Wolf-Rayet stars (WR), Be stars, AeBe stars, cataclysmic variables (CV), Mira stars, weak and classical T Tauri stars (WTT,ClTT), young stellar objects (YSO)).

The paper is organized as follows: new 2MASS/AllWISE DCCDs are generated and presented in Section 2. The results from a machine learning approach, classification tree, linear discriminant analysis (LDA) and K-nearest neighbours (KNN), are presented in Sections 3 and 4. In Section 5, we apply our classification criteria to a compilation of candidate SySts. This compilation includes candidates from the list of candidates (Paper I), the IPHAS (Corradi et al. 2008; Drew et al. 2005) and the VPHAS+ (DR2; Drew et al. 2014) surveys. A number of new very likely SySts candidates are presented. We finish with our conclusions in Sect. 6.

2 DIAGNOSTIC COLOUR-COLOUR DIAGRAMS (DCCD)

The 2MASS J–H vs. H–K_s DCCD has extensively been used to study the near-IR properties of SySts, to classify them into S- and D-types or to identify new candidates (Allen & Glass 1974; Rodriguez-Flores 2006; Phillips 2007; Corradi et al. 2008, 2010; Baella, Pereira & Miranda 2013; Baella et al. 2016; Clyne et al. 2015).

Corradi et al. (2008) propose two specific regions in which the majority of the S- and D-type are placed. Few years later, these regions were redefined by Rodriguez-Flores et al. (2014) being more restricted. In the J–H vs. H–K_s DCCD from Corradi et al. (2008), one can see that there is a small overlap between the S- and D-types probably because of some mis-classifications. The same overlap is not observed in the DCCD from Rodriguez-Flores et al. (2014) due to the preliminary selection of SySts from the IPHAS r–H α vs. r–i DCCD and the likely better classification by the authors (see Fig. 1 in Rodriguez-Flores et al. 2014).

Table 1. List of references for all the classes of objects.

Class of Object	Sample	References
PNe	188	Ramos-Larios & Phillips 2005
Post-AGB	180	Vickers et al.2015,Akras et al.2017
		Suarez et al. 2006, Yoon et al. 2014
Wolf-Rayet	162	van der Hucht 2001
Be	185	Chojnowski et al. 2015
AeBe	173	Vieira et al. 2003,
		Herbst & Shevchenko 1999
		Rodrigues et al. 2009
CV	191	Hoard et al. 2002
Mira	316	Huemmerich & Bernhard 2012,
		Whitelock et al. 2008
K giants	240	Carlberg et al. 2011, Gray et al. 2016
M giants	210	Tabur et al. 2009, Gray et al. 2016
Classical T Tauri	183	Galli et al. 2015, France et al. 2014
		Grankin et al. 2007,
		Herbst & Shevchenko 1999
Weak T Tauri	213	Grankin et al. 2008, Galli et al. 2015
		Cieza et al. 2007,
		Herbst & Shevchenko 1999
YSO	260	Rebull et al. 2011, Harvey et al. 2007
SySts	220†	Paper I and references therein

† Galactic SySts

In Figure 1, we present the 2MASS J–H vs. H–K_s DCCD for all the known Galactic SySts. For the vast majority of them, the classification is based on the SED profiles (Paper I), whereas for those without an SED profile and thus a new classification, the old one has been considered. Besides SySts, various classes of objects that show H α emission such as PNe, WR stars, Be and AeBe stars, CVs, Mira stars, CTT and WTT stars as well as post-AGB stars and single K-M giants are also included.

The sample size of all these classes of object as well as the references are given in Table 1. The photometric magnitudes were obtained from the AllWISE (Cutri et al. 2014) and 2MASS (Cutri et al. 2003) catalogues using a searching radius of 6 arcsec due to the resolution of the *W3* and *W4* bands. For approximately 90 per cent of the sources, the cross-matching of the 2MASS and AllWISE was made in a radius less than 1 arcsec. Only sources with actual measurements and no upper limit values were selected for all the classes of objects except CV[1].

Genuine PNe often mimic SySts mainly in the optical regime. In the 2MASS J–H vs. H–K_s DCCD, the majority of PNe are found to be bluer in the H–J colour index (<0.9) compared to SySts (>0.8) occupying the lower part of the

[1] By verifying various catalogues of CVs, we found that the vast majority have only upper limit magnitudes in *W3* and *W4*. Moreover, more than 95 per cent of CVs have J–H colour index lower than 0.75 which means that the upper limit values magnitudes in *W3* and *W4* do not affect our classification tree model (see § 3, Figure 7 and Figure A3). Therefore, we decided not to excluded the CVs with upper limit *W3* and *W4* magnitudes in order to keep their sample size comparable with the rest of the mimics and the sample size of SySts.

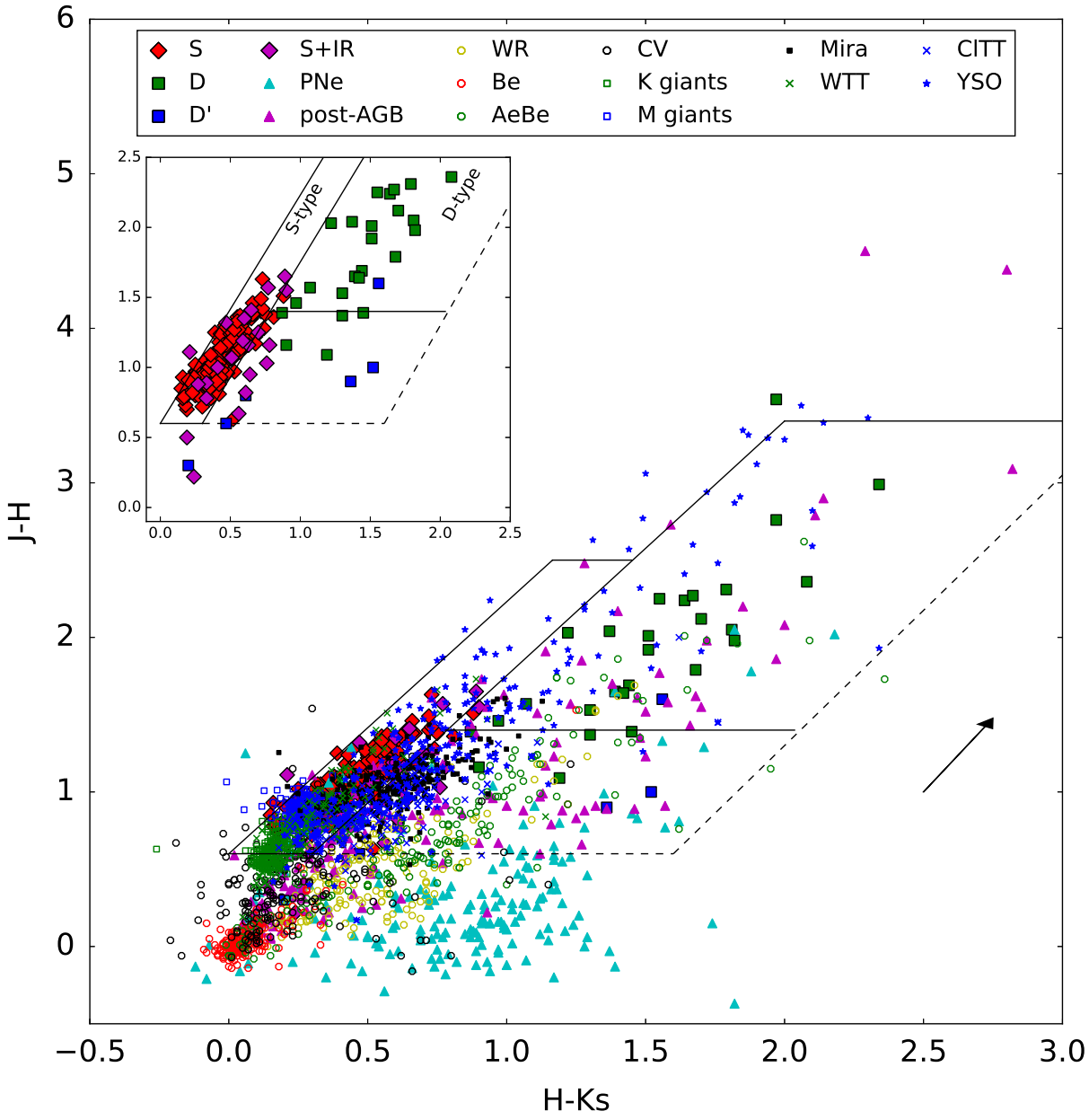

Figure 1. The 2MASS J–H vs. H–K_s DCCD for different classes of objects. The same DCCD for the four type of SySts is presented in the inset plot. The dashed and solid boxes define the regimes of S- and D-type SySts from Corradi et al. (2008) and Rodrígues-Flores et al. (2014). The black arrow corresponds to 4 mag extinction in the V band. The names in the box correspond to S-, D-, D′- and S+IR-type SySts, planetary nebulae (PNe), post-AGB stars (post-AGB), Wolf-Rayet stars (WR), Be stars (Be), AeBe stars (AeBe), cataclysmic variables (CV), K/M giants, weak/classical T Tauri stars (WTT/ClTT) and YSO.

DCCD. However, there is small number of PNe with H–J>0.9 that are mixed up with S- and D-type SySts. These are likely denser and younger members. On the other hand, post-AGB, YSO and AeBe stars are found to be well mixed with the D-type SySts. *This clearly illustrates than the dusty SySts cannot easily be distinguished from other dusty sources in the near-infrared wavelength regime.* In the left part of the plot with 0<H–K_s<1 (Fig. 1), we find the locus of S-type SySts as well as a number of other sources such as single M and K type giants, WTT and ClTT stars and Mira stars. All these sources are well mixed making hard to distinguish them based only on the 2MASS colours. The single K and M

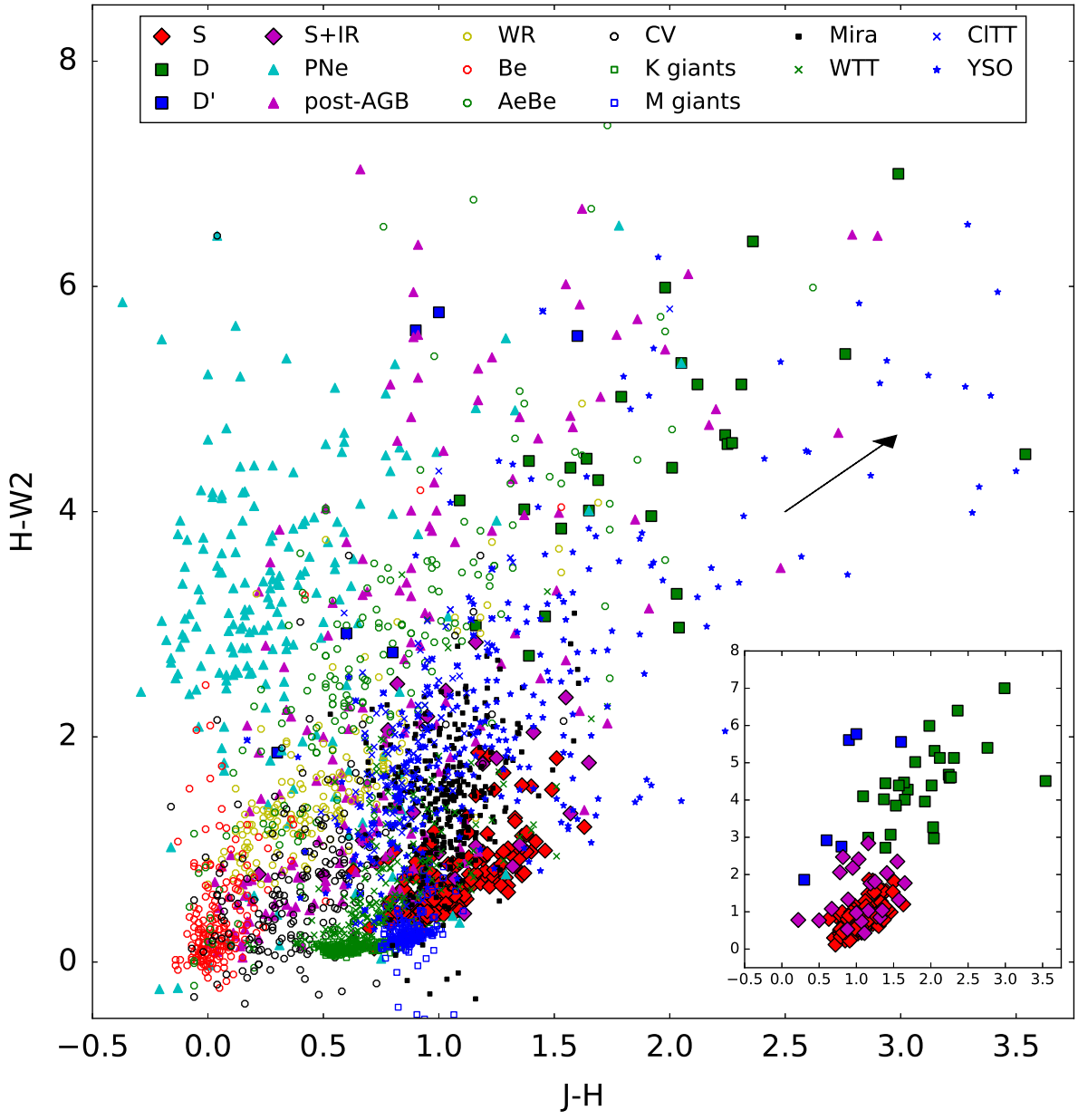

Figure 2. The 2MASS/AllWISE *H–W2* vs. *J-H* DCCD for different classes of objects as well as for the four type of SySts presented in the inset plot. The black arrow corresponds to 4 mag extinction in the *V* band.

type red giants are found to be bluer in the *J–H* colour index (<1) compared to the S-type SySts with a cool companion of the same spectral type (see also Catchpole & Glass 1974). A similar behaviour is also found between the single Mira stars and D-type SySts. This may be associated with a higher dust formation rate in SySts than in single giants. Evidence of fast rotation in some S-type SySts and the majority of D′-types compared to single giants may indicate a substantial increase in mass-loss rate by a factor of 10 (Zamanov et al. 2006, 2008) or the higher mass-loss rate of symbiotic Mira stars compared to normal ones (Gromadzki et al. 2009). WTT and ClTT stars appear to occupy different areas in this DCCD. WTT are well mixed with S-type SySts while ClTT show a redder $H–K_s$ colour index. The bulk of WR stars is found to occupy a region between SySts and PNe. However there is a small number of WR stars which exhibit similar colour indices with the D- and D′-type SySts.

In the inset plot, we display for clarity only the four

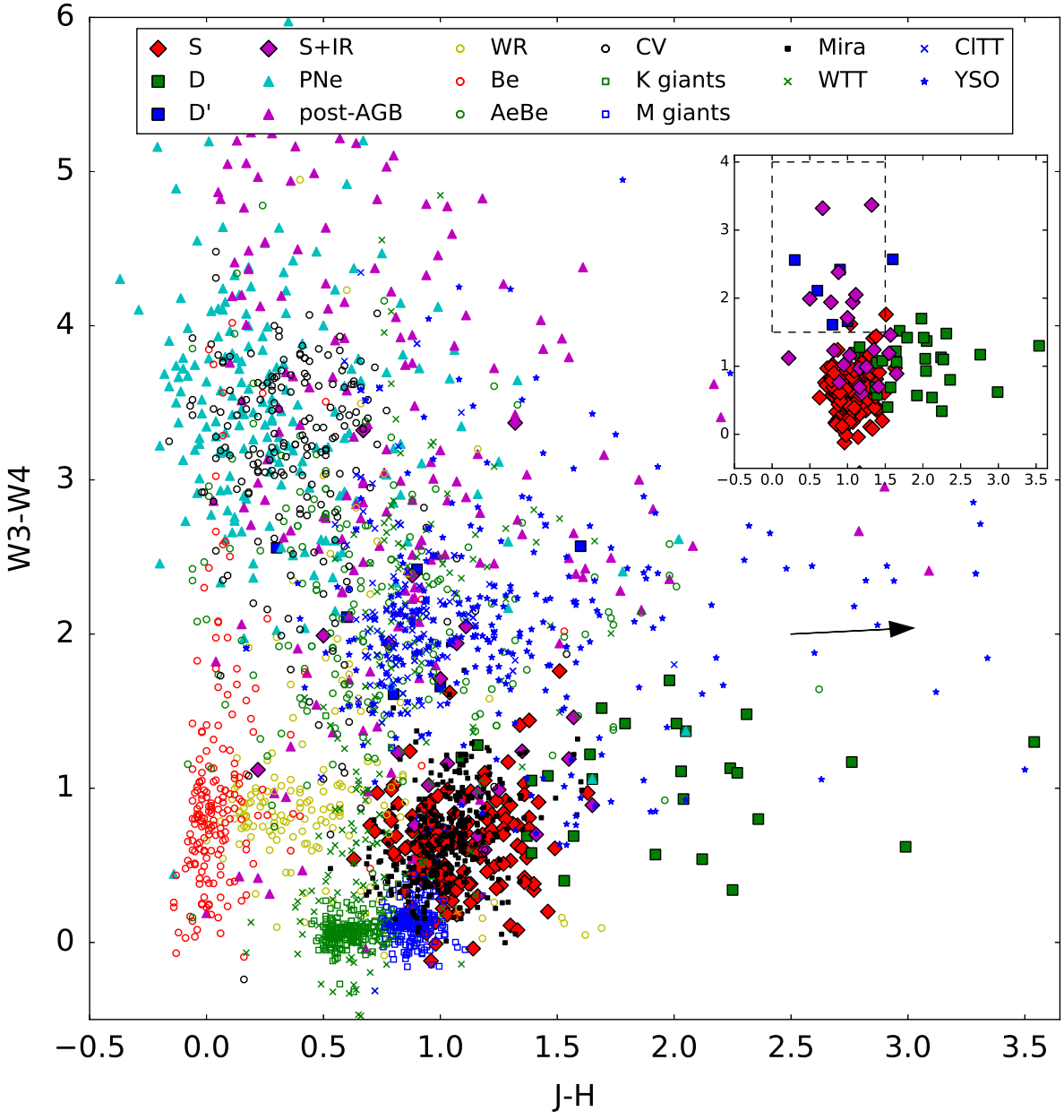

Figure 3. The 2MASS/AllWISE *W3*–*W4* vs. *J*–*H* DCCD for different classes of objects as well as for the four type of SySts presented in the inset plot. The black arrow corresponds to 4 mag extinction in the *V* band. The dashed box in the inset plot indicates the vertical branched region of SySts discussed in the text. The *W3* and *W4* magnitudes of the majority of CVs correspond to upper limit values.

types of SySts. There is a clear separation between the S and D types which agrees with the regions defined by Corradi et al. (2008) and Rodriguez-Flores et al. (2014). D′-type SySts are found to be highly dispersed in this DCCD without occupying any specific region with the *J*–*H* and *H*–K_s colour indices range from 0 to 1.75. The new S+IR-type SySts (see definition in Paper I) are found to lie in the same region as the S-type. This is not surprising since the only difference between the S- and S+IR-types is, by definition, an infrared excess at longer wavelengths (11.6 and 22.1 μm), which explains why they have not been recovered before.

The *J*–K_s vs. *Y*–*J* DCCD has also been reported for distinguishing SySts from PNe (Miszalski et al. 2011). D-type lie in different region from S-type based on the *J*–K_s colour index (S-type:≤2.20; D-type:≥2.20) equivalently to the *J*–*H* colour index.

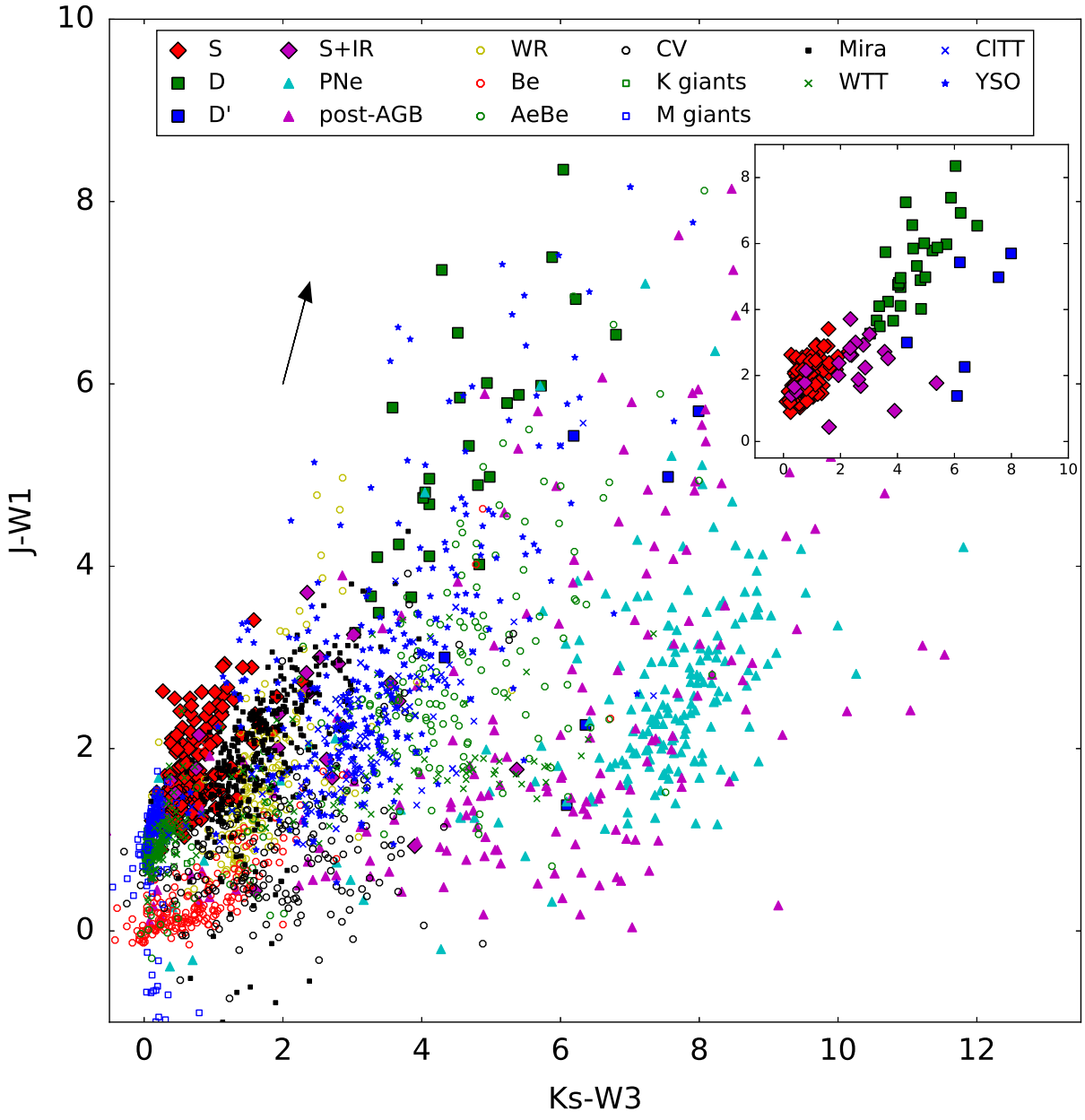

Figure 4. The 2MASS/AllWISE *J–W1* vs. K_s*–W3* DCCD for different classes of objects as well as for the four type of SySts presented in the inset plot. The black arrow corresponds to 4 mag extinction in the *V* band. The *W3* magnitude of the majority of CVs corresponds to upper limit values.

Besides the common *J–H* vs. *H–*K_s DCCD, we explored all the possible DCCDs using all the different combinations between 2MASS and AllWISE data. We present, here, the most representatives DCCDs that provide a good separation among the different classes of objects: *H–W2* vs. *J–H* (Fig. 2), *W3–W4* vs. *J–H* (Fig. 3), *J–W1* vs. K_s*–W3* (Fig. 4), *J–H* vs. *W1–W4* (Fig. 5) and *W3–W4* vs. K_s*–W3* (Fig. 6).

The *H–W2* vs. *J–H* DCCD (Fig. 2) provides a better separation among the different type of objects than the previous one. Mira and WTT stars, which are well mixed with the S-type SySts in the previous DCCD, are found to be redder in the *H–W2* colour index compared to the bulk of S-type and bluer compared to the D and D′-ype SySts. PNe, post-AGB, YSO, D- and D′-type SySts have the same range of *H–W2* colour index (from 2 to 7) but different *J–H* colour index – PNe are bluer and occupy the upper-left part, YSO are

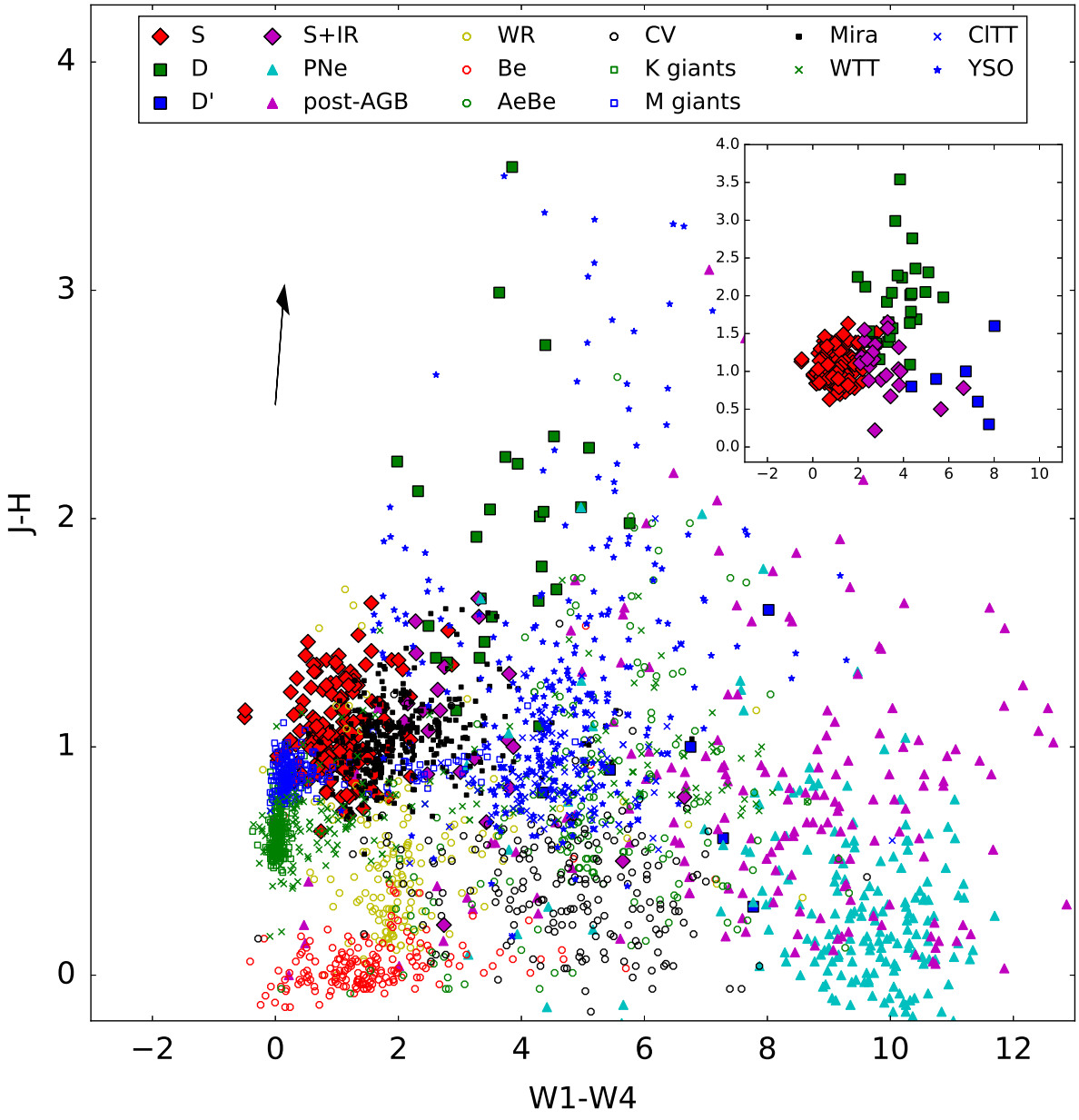

Figure 5. The 2MASS/AllWISE *J–H* vs. *W1–W4* DCCD for different classes of objects as well as for the four type of SySts presented in the inset plot. The black arrow corresponds to 4 mag extinction in the *V* band. The *W4* magnitude of the majority of CVs corresponds to upper limit values.

redder occupying the upper-right corner, while post-AGB, D and D′-type SySts are well mixed and occupy the region between PNe and YSO. Previous studies have shown that D′-type SySts have SEDs that resemble those of post-AGB stars. Be, WR, CV and M/K giants are located in the lower-left corner of the DCCD.

Miszalski et al. (2011) argue that *J* –[4.5] colour index is ideal for separating PNe and H II regions from SySts with the former having *J* – [4.5]<4 and the latter >5 (see Fig. 7 in Miszalski et al. 2011). At least for the Galactic SySts, we find that the *J* – *W2* colour index (not presented here, or equivalently *J* – [4.5]) alone is not a good indicator for identify SySts as a significant number of PNe also exhibit *J* – [4.5]>5. Reid (2014) also find the same result for PNe in the LMC.

The *W3–W4* vs. *J–H* DCCD (Fig. 3) provides a good

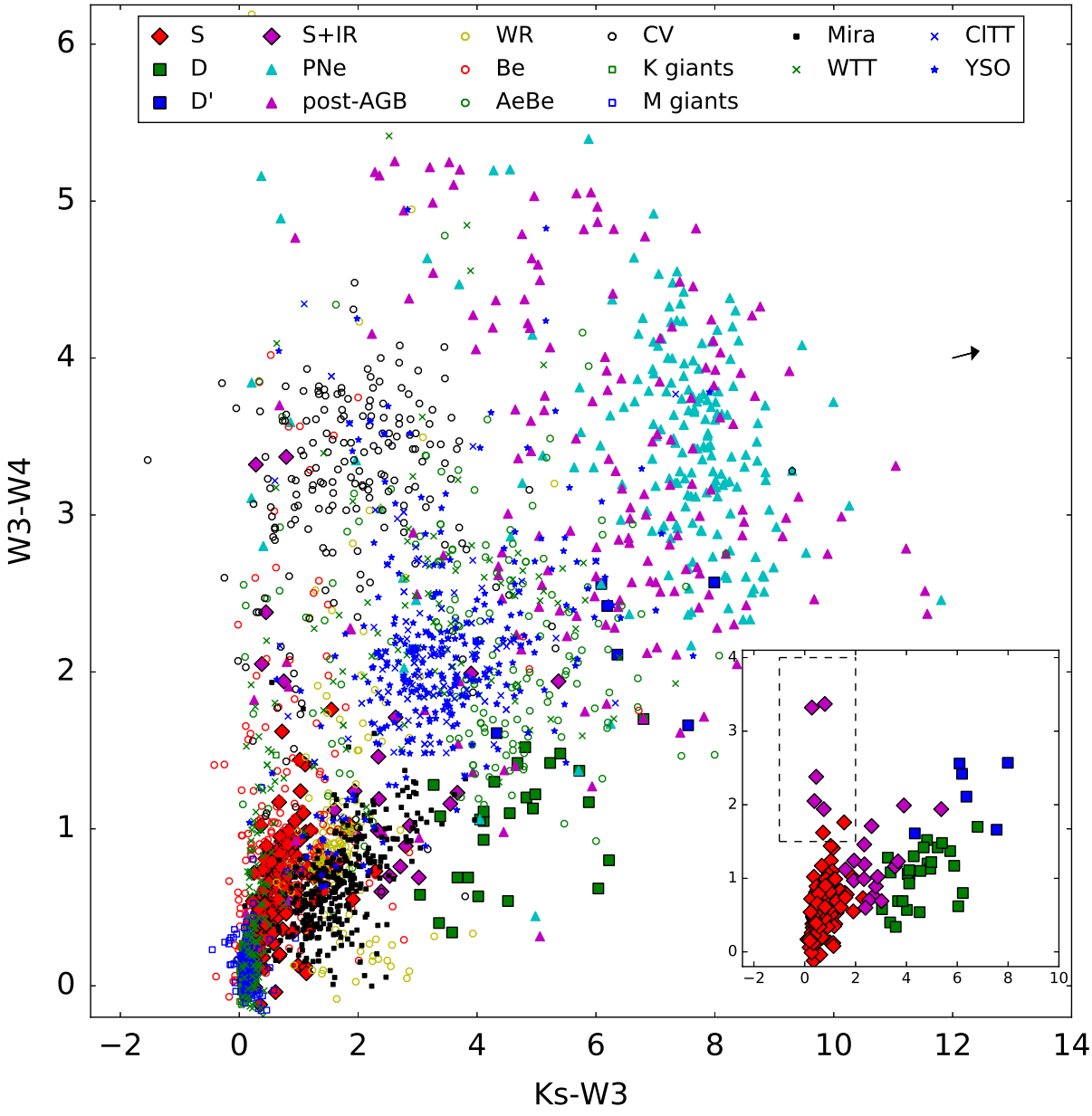

Figure 6. The 2MASS/AllWISE *W3*–*W4* vs. K_s–*W3* DCCD for different classes of objects as well as for the four type of SySts presented in the inset plot. The black arrow corresponds to 4 mag extinction in the *V* band. The dashed box in the inset plot indicates the vertical branched region of SySts discussed in the text. The *W3* and *W4* magnitudes of the majority of CVs correspond to upper limit values.

separation of SySts from other types of objects. In particular, D-type SySts are found to be located in the bottom-right corner of the DCCD while PNe/post-AGB stars are found in the upper-left corner and YSO in the centre of the plot. S-type are also well separated from sources like WTT, ClTT, K and M giant, Be and CV but not from Mira stars.

From this DCCD, we conclude that *W3*–*W4* colour index is a good indicator for SySts with the vast majority of them displaying 0< *W3*–*W4*<1.5. Although, there is a small number of SySts with values between 1.5 and 4 (dashed-line box). These objects deserve a further study in order to reveal their true nature and understand why they display higher *W3*–*W4* colour index while the *J*–*H* is nearly constant (see also Fig. 6). The possibility of unreliable *W3* and *W4* photometric magnitudes cannot be ruled out given that one SySt has photometric errors higher than 0.1 dex (UKS Ce-1).

The *J–W1* vs. K_s*–W3* DCCD (Fig. 4) also separates the different classes of objects as well as the four types of SySts. In particular, the majority of S+IR-type SySts are found to occupy a specific region between the S- and D-types. This may suggest that the S+IR-type are a transition type between the S- and D-type SySts. The intriguing D′-type SySts have lower *J–W1* and higher K_s*–W3* colour indices compared to D-types but similar to those of post-AGB and PNe. Again, D-type SySts and YSO are found to occupy the same regime. Moreover, Mira stars and D-types seem to form a continuous branch in which D-type are redder in both colours than single Mira stars due to the dusty shells around the binary systems in SySts. This agrees with the hypothesis that Mira stars in SySts have higher mass-loss rate compared to normal Mira stars (Gromadzki et al. 2009). S-type SySts (bluer in K_s*–W3*) are found to be well separated from Mira stars (redder in K_s*–W3*) in this DCCD.

In the following DCCD (*J–H* vs. *W1–W4*, Fig. 5) S-, S+IR-types and Mira are located in a region with *J–H*∼1 and 0< *W1–W4*<4. D-type, on the other hand, are clearly distinguished from all other objects having *J–H*>1.25 and 3< *W1–W4*<6. The common mimics of D-type SySts, PNe and post-AGB, are located in the bottom-right corner of the DCCD. D′-type SySts have colour indices similar to those of PNe and post-AGB and occupy the same region. The systematically low *W1–W4* colour index of D-type is attributed to a weaker emission in the 22μm relative to D′-type, PNe and post-AGB stars.

The last DCCD, *W3–W4* vs. K_s*–W3*, (Fig. 6), provides the best separation among the four types of SySts covering different values ranging K_s*–W3*. In particular, S-, S+IR-, D- and D′-type SySts exhibit K_s*–W3*<2, 2<K_s*–W3*<3, 3<K_s*–W3*<6 and K_s*–W3*>6, respectively. K_s*–W3* index is, thus, a good indicator for an infrared excess or the presence of a dusty shell. Regarding the other classes of objects, D-type SySts are very well separated from all the dusty sources like PNe, post-AGB, YSO and AeBe with very little contamination. D′-type are still hard to be separated from post-AGB and PNe.

S-types are well distinguished from WR and Mira stars which are found to be redder in the K_s*–W3* colour index by approximately 1 dex. However, S-type are strongly contaminated with Be, WTT and K/M giants. The vertical branch of S- and S+IR-type SySts becomes apparent in this DCCD similar to Figure 6 (bashed box in the inset plot). SySts in that region display *W3–W4*>2.0 occupying the same locus with CVs. From Figure 6, one can see that *W3–W4* increases with the increase of K_s*–W3* (e.g. blue square symbols for D′-type SySts). We conclude that SySts with *W3–W4*>2.0 in the vertical branch of Figure 6 are likely more dusty or the photometric data are uncertain. We argue that a more careful study of these specific S- and S+IR-type SySts is necessary. It is also worth mentioning that this DCCD is equivalent to the IRAS K-[12] vs. [12]-[25] DCCD from Luud & Tuvikene (1987) who argued that it can identify the S-, D- and D′-type SySts.

By cross-matching the WISE and *Kepler-Isaac Newton Telescope Survey* (KIS, Greiss et al.2012) catalogues, Scaringi et al. (2013) demonstrate that CVs occupy a specific region in the *W1–W2* vs *W2–W3* and *W1–W2* vs *W3–W4* DCCDs well separated from quasi-stellar objects (QSOs). Despite the low number of CVs, it seems that they exhibit *W2–W3*>1 and *W3–W4*>2.75. Our *W3–W4* vs. K_s*–W3* DCCD also provides the same result with the CVs lying in the region of 2.5< *W3–W4*<4. But, most of the CVs have only upper limit *W3* and *W4* magnitudes which make their position quite uncertain.

We also conclude that CVs, S- and S+IR SySts have *W1–W2* colour index between 0 and 0.4 in agreement with Debes et al. (2011). In particular, CVs have an average *W1–W2* colour index equal to 0.16 with a standard deviation of 0.24, S-type have an average value of 0.02 (SD=0.16) and S+IR-type have an average value of 0.37 (SD=0.32). Given that CVs, S- and S+IR SySts are composed of a white dwarf (WD), their *W1–W2* values are consistent with Debes et al. (2011) for single white dwarfs. Regarding D-, D′-type SySts and PNe, which are also composed of a WD, we find systematically higher *W1–W2* colour index of 1.12 (SD=0.43), 1.16 (SD=0.45) and 0.91 (SD=0.46), respectively. Dust emission in these specific classes of objects is strong enough to overwhelm the emission from the WDs resulting in higher colour index compared to the stellar SySts and CVs.

Overall, these new 2MASS/AllWISE DCCDs provide essential information for studying SySts as well as distinguish them from other stellar objects. *J–H* vs. *H–*K_s, *H–W2* vs. *J–H* and *J–W1* vs. K_s*–W3* DCCDs provide a good separation among SySts, PNe, YSO and post-AGB stars. The last two DCCDs also separate S-type SySts from Mira stars. The *W3–W4* vs. *J–H* and *J–H* vs. *W1–W4* DCCDs can distinguish SySts from mimics like CVs, WR, WTT, ClTT star, Be stars and single K and M giants.

The K_s*–W3* vs. *W1–W4* DCCD has been proposed to separate very well SySts from PNe and ClTT stars, but only once sources like Mira, CVs, Be stars have already been discarded from the samples based on their Hα emission i.e. *r–i* vs. *r*–Hα IPHAS DCCD (Corradi private communication).

It should be noted that none of the previous DCCDs provide an adequate separation between the D′-type SySts and PNe occupying the same regions on these IR DCCDs. On the other hand, D-types are better distinguished (e.g. *J–H* vs. *H–*K_s or *J–H* vs. *W1–W4*).

This difference between the D′- and D-type SySts is likely associated with the progenitor of the circumstellar nebula around these systems: (i) the hot WD companion when entered in the AGB phase (D′-type) or (ii) the cold giant companion (D-type) (Schwarz & Corradi 1992; Munari & Patat 1993; Pereira, Smith, Cunha 2005). According to the first scenario, a D′-type SySt can also be consider as a genuine PNe since the circumstellar envelope has been expelled by the same star than ionizes it, while the second scenario implies that the circumstellar evelope, ionized by the WD, is the material lost by the cold giant and transferred to the WD. Therefore, there may exist objects with a dual nature, classified either as SySts or PNe with a binary central system.

3 CLASSIFICATION TREES

DCCDs are widely used to distinguish different classes of objects as well as to find new candidates. However, in order to perform a more quantitative analysis and derive the criteria that can easily be used, the machine learning algorithm of classification tree is used (Moret 1982, Buntine 1993).

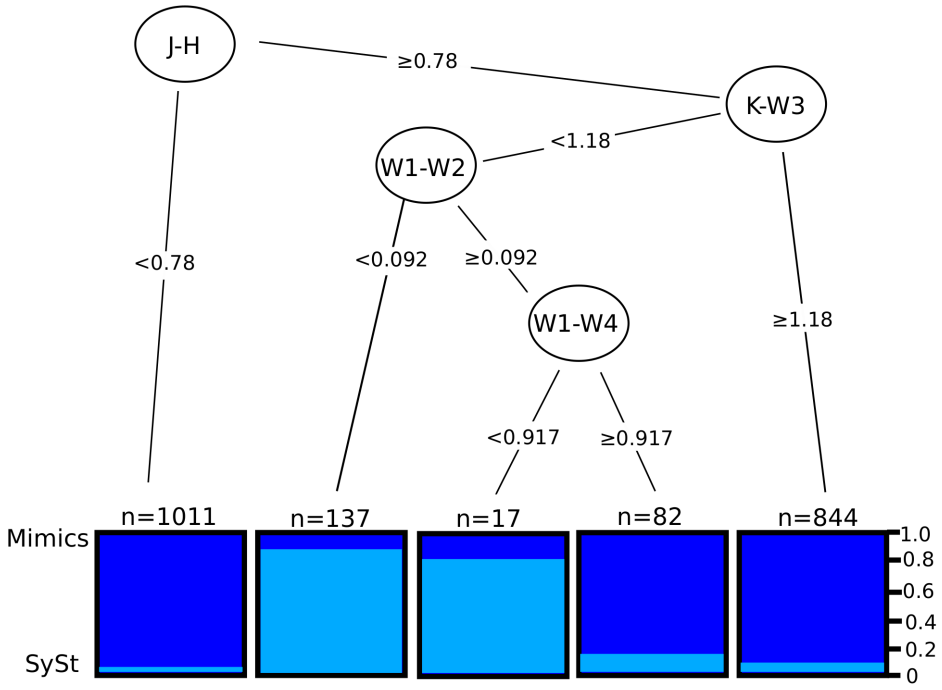

Figure 7. Classification tree plot using as training sample the groups of all known Galactic SySts and the mimics. Each column represents the population of the sources (normalised to one) that satisfy the colour criteria and the total numbers of these objects is given at the top of each column. The sum of the population in each column or criterion corresponds to the total population of the training sample. The colour criteria are given inside the ellipses. The dark and light blue colours correspond to the sample of the mimics and SySts, respectively.

In astrophysics, the classification tree method has been applied to set of observable parameters in order to derive the criteria that provide the lowest contaminated groups (e.g. da Silva, Milone & Rocha-Pinto 2015). For this analysis, the evtree function (Grubinger, Zeileis & Pfeiffer 2011) in R software R was used with a set of 10 representative colour indices (*J–H*, *H–K*$_s$, *K*$_s$*–W1*, *W1–W2*, *W2–W3*, *W3–W4*, *W1–W4*, *J–W1*, *H–W2* and *K*$_s$*–W3*).

As a training sample for our classification tree model, we used all possible sources that mimics SySts in the optical regime i.e. Hα emitters, as the criteria to identify SySts are based on information in the optical wavelengths (see Kenyon 1986; Mikolajewska, Acker, Stenholm 1997; Belczynski et al. 2000). There are several classes of objects that show Hα emission like SySts, but we selected only the bright ones such as PNe, WR, Mira, CVs, YSO, ClTT, WTT, AeBe and Be sources (see also Witham et al. 2006, Corradi et al. 2008) which satisfy the IPHAS criterion (*(r-H*α*)*$\geq$ *0.25*$\times$*(r-i)+0.65*, Corradi et al. 2008) and it is applied to the IPHAS and VPHAS+ catalogues to get the final samples (see Section 5).

Late K or M dwarf stars as well as main sequence stars and red giant stars also show Hα emission. However, it is generally very weak and all these sources can be easily distinguished from SySts (see Corradi et al. 2008). Supergiants are also Hα emitters but according to their synthetic *r-H*α and *r-i* colour indices (Drew et al. 2005), they occupy a totally different in the IPHAS diagnostic diagram. Therefore, we decided not to include them in our training sample, since the IPHAS criterion will automatically excluded them from our validate samples.

We also excluded H II regions and QSOs, two known Hα emitters for two reasons: (i) our analysis is focused on the Milky way and H II regions can be easily distinguished from compact SySts by looking at the observed images and (ii) the prior star/galaxy separation in photometric surveys minimises the contamination from QSOs. We should note here that in extragalactic surveys of SySts, the contamination of H II regions (or diffuse ionized gas, Mikolajewska et al. 2017) is significant and it has to be taken into consideration.

The main goal of this work is to reveal the hidden SySts population in Hα photometric surveys like IPHAS, VPHAS+, *the Javalambre Physics of the Accelerating Universe Astrophysical Survey* (J-PAS, Benitez et al. 2014), *the Javalambre Photometric Local Universe Survey* (J-PLUS, Cenarro et al. 2018, submitted) and *the Southern Photometric Local Universe Survey* (S-PLUS, Mendes de Oliveira et al. submitted), among others, taking into considerations, apart from the Hα excess, the 2MASS and AllWISE data.

Table 1 lists the most common mimics of SySts that may occupy the same area in the *(r-H*α*)* vs *(r-i)* DCCD (Corradi et al. 2008) as well as their sample sizes and the references. All the mimics have sample sizes approximately equal to the population of known Galactic SySts with no upper limit values (220). As we are interested in searching for the criteria that separate better SySts from all the mimics in Table 1, we merged their samples into one sample, namely "Mimics". This yields to a training sample of 220 SySts and 1871 mimics or in other words imbalanced training samples. This is a well known problem in data mining (e.g. He & Garcia 2009). Given that our goal is to identify

the minority class (SySts), it may impose a bias to the resulting model toward to the majority class. A few methods have been developed to overcome the imbalanced learning problem such as oversampling, undersampling or synthetic sampling among others (e.g. Weiss & Provost 2003; He & Garcia 2009; Longadge, Dongre, Malik 2013 and references therein).

In our case, the *between-class imbalance* of our training sample is of the order of 8.5:1, which is not such high but at the same time enough to be considered as imbalanced. If a training sample that represents the real population of SySts and mimics in the Milky Way is constructed, it may result in a significantly higher *between-class imbalance* and presumably to a poorer classification model biased towards the mimics. In addition to that, the true Galactic population of SySts (between 2000 and 400000) as well as of mimics are not very accurate and may provide less representative and more problematic training samples. It has been demonstrated that training samples with small sizes can also provide good classification models as training samples with bigger sizes (Weiss & Provost 2003).

By keeping constant the sample size of mimics and randomly reducing the sample size of SySts to 50, 100 and 150, or in other words increasing the *between-class imbalance* to 38:1, 19:1 and 13:1, respectively, we found that the colour criteria change no more than 8-9 per cent relative to the values in Figure 7. The lower the size of SySts the high the difference. For instance, the low prevalence of S+IR-type SySts in the training samples results in lower $W1-W2$ colour. This is a characteristic example of training samples that suffer from lack of information (Visa & Ralescu 2005). Recall that we are interested in the minority class of SySts, their whole sample size of 220 sources provides all the available information of this class of objects.

By replicating the sample of SySts a few times (oversampling method), the distribution of SySts in various colour indices becomes significantly different compared to the distribution of mimics. For instance, the numbers of D-types and D′-type substantially increase relative to the number of dusty mimics like YSO and PNe. Equivalently, if we randomly reduce the number of mimics (undersampling method), we may get significantly less Miras, WTT or ClTT star relative to S-type SySts. Because of the small number of known SySts, these two methods of re-sampling the training samples are not ideal.

Despite our models are eventually trained using imbalanced samples, the construction of the training samples with equal populations for all classes of mimics and SySts assures that they are unbiased towards any of these sources.

Classification tree was also applied to several training samples with three different classes of objects each in order to derive those colour criteria that identify SySts among various classes of objects. A training sample with the four types of SySts (S-type/S+IR-type/D-type/D′-type) was also used to train our model in order to seek for the colour criteria that can separate these four types.

Figure 7 displays the classification tree plot using as a training sample the group of all the known Galactic SySts (light blue) and mimics (dark blue). The majority of SySts can be distinguished from their mimics using the $J-H$, K_s-W3, $W1-W2$ and $W1-W4$ colour indices. Almost 50 per cent of the population of mimics (1011 sources) exhibit $J-H<0.78$ while SySts appear to have $J-H>0.78$. This first group contains mainly Be, CV, PNe WR, and WTT as well as a small number of S-type SySts with $J-H<0.78$ (10 sources). The second criterion $K_s-W3<1.18$ separates SySts from the remaining mimics. However, there is a number of SySts (62 sources) that exhibit $K_s-W3>1.18$ and they are misclassified. These SySts are mainly the dusty ones like S+IR-, D- or D′-type. From the DCCDs above, we have shown that the dusty SySts are well mixed with YSO, PNe, and AeBe stars and they are very hard to be distinguished. The third and forth criteria give us all the remaining S-type SySts. In particular, 137 S-type SySts or 83 per cent satisfy the criterion $W1-W2<0.092$ with 10 per cent contamination[2], whereas 15 S-type pass the fourth criterion $W1-W4<0.917$ with 15 per cent contamination. In total, these two criterion give us 93 per cent of the S-type SySts and they are mainly contaminated with K/M giants, WTT and Mira stars. Overall, we argue that these four colour criteria can be used to distinguish and identify S-type SySts with an accuracy up to 90 per cent.

In order to find the right colour criteria that distinguish the dusty SySts (S+IR, D and D′), we used as a training sample the subgroup of the dusty SySts and the sample of mimics (Figure 8). Two criteria $H-W2>3.806$ and $W1-W4<4.715$ are found to provide the best combination for identifying dusty SySts. However, these colour criteria are not as good as the previous ones of S-type for two reasons: (i) only 25 SySts or 45 per cent satisfy both criteria and (ii) the high contamination of 25 per cent with other classes of objects. Examining all the dusty SySts one by one, we conclude that the criteria works only for the D-type SySts. The S+IR have $H-W2<3.806$ and the D′-type $W1-W4>4.715$ being misclassified (see also Fig. A6).

The overall accuracy of the algorithm was verified by randomly selected 80% of the Galactic SySts sample as training set and 20% as testing set and repeated it for a few times. We find an accuracy range from 71% to 77% while the values of the criteria vary from 5 to 8%. The low accuracy of our model is attributed to the dusty SySts which cannot be distinguished from other dusty sources (e.g. PNe, YSO). Hence, we repeated the same procedure but this time the testing set was generated by randomly selected 20% from the S-type SySts. In this case, the accuracy of the method becomes higher from 82% to 88%. Moreover, the false identifications were found to be around 1% for the mimics and 13% for the S-type SySts.

Figure 9 displays the classification tree plot for the four types of SySts (S, S+IR, D and D′). The K_s-W3 is the principal criterion that distinguishes the stellar from the dusty SySts. The left branch includes those SySts that are bluer in the K_s-W3 (<1.93) and they are divided into two subgroups: the S-type with $W3-W4<1.46$ (163 sources or 99 per cent) suffering of only 0.5 percent contamination from S+IR and the S+IR-type with $W3-W4>1.46$ (5 sources or only 22 per cent) suffering of 29 per cent contamination from S-type. The right branch ($K_s-W3>1.93$) contains mainly all the dusty SySts. The S+IR-type have $H-W2<2.72$ with 11 per cent contamination (one S-type and one D-type) whereas

[2] the contamination levels are given relative to the total number of objects that satisfy a specific criterion

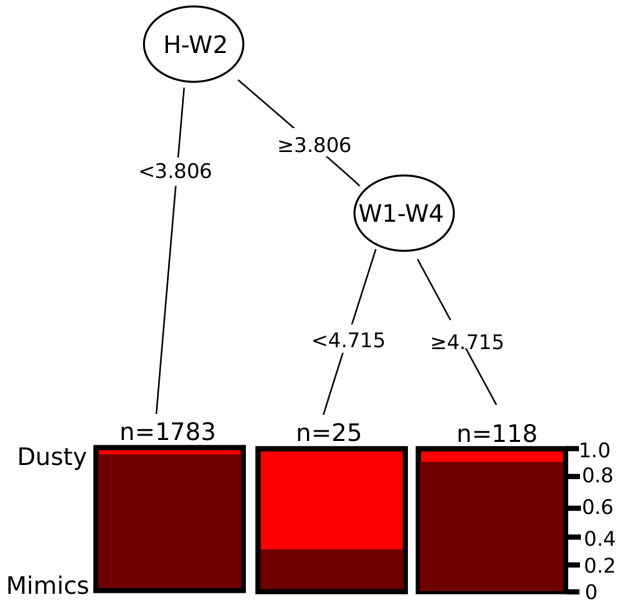

Figure 8. Classification tree plot using as training sample the groups of all dusty (S+IR, D and D′) known Galactic SySts and all the mimics.The dark and light red colours correspond to the sample of the mimics and dusty SySts, respectively.

the more dusty SySts (D and D′) have *H–W2*>2.72 (i.e. strong infrared excess) and they are further separated by the *W3–W4* colour (D-type: *W3–W4*<1.52 (97 per cent); D′-type: *W3–W4*>1.52 (86 per cent)).

Evidently, the *H–W2* and *W3–W4* indices are strong indicatives for the presence of a dusty shell in SySts and likely in any other dusty sources (see Fig. 8). Moreover, if we take the S+IR-type SySts out from this analysis as well as the *H–W2* colour index criterion, the classification tree yields as the best indicators the K_s*–W3* and *W3–W4* colour indices. This is the result in which Luud & Tuvikene (1987) concluded using the IRAS colours – K-[12] and [12]-[25] – which are equivalent to our colour criteria.

Figure 10 illustrates a 3D colour plot among the most relevant colour indices according to the results from the classification tree algorithm. The four SySt types can be better illustrated in this 3D colour diagram than the previous 2D DCCD. S+IR-type SySts are vividly occuping a different region between the S- and D-type SySts, whereas two distinct locus are also defined for the D- and D′-types SySts.

We then used the following training samples with different classes of source in order to find those criteria that distinguish SySts from specific classes of sources: (i) SySts/PNe/Be, (ii) SySts/CV/Mira, (iii) SySts/CV/YSO, (iv) SySts/WR/post-AGB, (v) SySts/K-giants/M-giants, (vi) SySts/WTT/ClTT, (vii) SySts/Be/AeBe. The first training sample includes SySts, PNe and Be (see Fig. A1), two of the most common mimic of SySts due to the emission of several common lines. The first *W1–W4* colour index criterion discriminates SySts and Be stars from PNe. Almost all PNe (166 sources or 88 per cent) satisfy the criterion *W1–W4*>7.285 while they suffer by a 3 per cent contamination from Be and SySts. Interestingly, all SySts are D′-type, a further proof that D′-type SySts do resemble PNe. It is worth mentioning that except one D′-type SySt (K 5-33) none of them emit the O VI λ6830 Raman-scattered line, which is a strong indicator of the symbiotic activity (Paper I). Therefore, an additional confirmation of this line in K 5-33 is necessary due to the low signal-to-noise ratio of its detection (Miszalski, Mikolajewska & Udalski 2013). Be stars and SySts exhibit lower infrared excess *W1–W4*<7.285 compared to PNe. 98 per cent of Be stars show *J–H*<0.541. On the other hand, 96 per cent of the known Galactic SySts show *J–H*>0.541 and *W3–W4*<2.56 suffering of only 3 per cent contamination. Finally, those nine sources (seven PNe, two SySts and one Be star) with *W3–W4*>2.56 deserve further study in order to explore possible link among them.

Figure A2 shows the classification tree plot between SySts, CV and Mira stars. At this point, we have to clarify that only a set of 6 colour indices were used in our classification tree model. Due to the upper limit magnitudes of CVs in *W3* and *W4*, we did not use the colours *W2–W3*, *W3–W4*, *W1–W4* and K_s*–W3*). SySts are separated into two groups depending on the *W1–W2* colour index. SySts with *W1–W2*<0.151 are classified as S-type and they are systematically redder in the *J–H* colour than CVs. On the other side, the dusty SySts exhibit *W1–W2*>0.151 but they are the minority compared with Mira stars and CVs which show clearly different *J–H* colours (CVs: *J–H*<0.684, Mira: *J–H*>0.684)).

The next training sample contains SySts, CV and YSO (Figure A3). In this case, CVs are easily separated from SySts and YSO based on the criterion *J–H*<0.663 and the upper limit magnitudes in *W3* and *W4* do not affect our model. SySts and YSO exhibit both *J–H*>0.663 and they are distinguished based on the K_s*–W3* colour. SySts with K_s*-W3*<1.344 correspond to S-type whereas those with *W3–W4*>1.344 correspond to the dusty SySts and are mixed with YSO.

SySts, post-AGB and WR stars can also be separated very well using the *J–H* and *W1–W4* colour indices (Fig. A4). The vast majority of post-AGB stars show *W1–W4*>4.735 and they are contaminated by only few WR

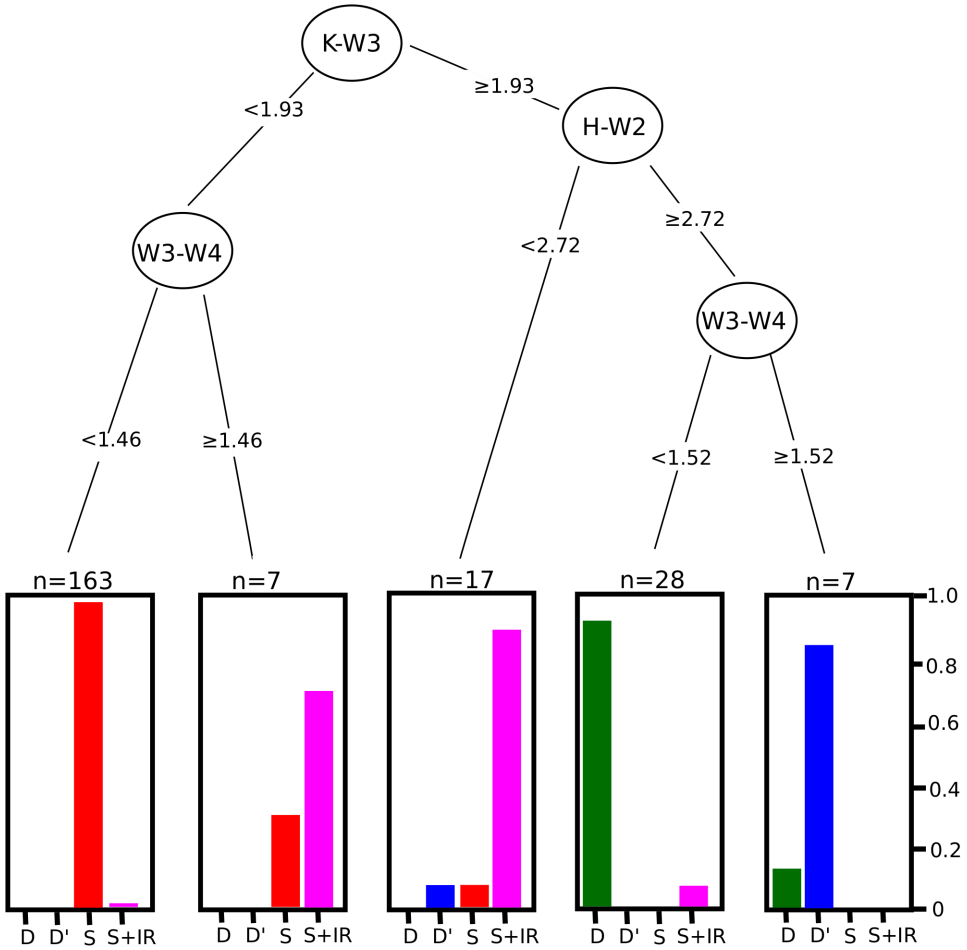

Figure 9. Classification tree plot using as the training sample the four types of SySts.

and SySts. SySts (92 per cent) are found to exhibit *W1–W4*<4.735 and *J–H*>0.774 while WR stars have *J–H*<0.774

In Figure A5, we present the classification tree plot for the training sample among SySts and M/K giants. Given that S-type SySts have a M or K giant companion, it is coherent to explore the colour indices that discriminate SySts from single M/K giants. Almost all SySts (95 per cent) have *H–W2*>0.206 and K_s*–W3*>0.27 with a very small contamination mostly from M giants and few K giants (3 per cent), which should be further investigated. Approximately 50 per cent of M giants show the same *H–W2* colour with SySts but are bluer in the K_s*–W3* colour index (<0.27). Regarding the K giants, the majority of them shows *H–W2* colour index <0.206 and they are separated from M giants based on the *W2–W3* colour index. A similar work using the *i*, *Y* or *Z* bands may be very useful for discriminating SySts and red giants.

The resultant classification tree plot among the SySts, WTT and ClTT is displayed in Figure A6. Almost all SySts have *W3–W4*<1.483 and *J–H*>0.78 and they suffer of only 5 per cent contamination. Half of WTT stars are found to be bluer in the *J–H* colour index (<0.78) compared to SySts. The remaining of WTT have *W3–W4*>1.483 and they are mixed with ClTT and few SySts. The *W1–W2* colour index separates further the WTT and the ClTT stars with the former being bluer and the latter redder.

AeBe stars also emit strong Balmer lines and mimic SySts in the optical regime. It is thus consistent to train our model with a training sample among SySts, Be and AeBe stars (Figure A7). The *W1–W4* colour index is the first criterion that strongly discriminated SySts and Be stars from AeBe stars. SySts and Be are found to be bluer in the *W1–W4* colour (<3.949) compared to the AeBe stars (>3.949). SySts and Be stars are further separated based on the *J–H* colour index (Be<0.63, SySts>0.63). The contamination of these two groups is small of the order of 5.9 and 1.7 per-cent, respectively. On the other hand, AeBe stars exhibit *W1–W2*>0.03 with a very small contamination of SySts and Be.

Overall, we conclude that primarily *J–H*, *W1–W4* and K_s*–W3* and secondarily *H–W2*, *W1–W2* and *W3–W4* colour indices provide the best combinations of colours for distinguishing SySts from their mimics. Classification tree is evidently a powerful statistical tool to separate/classify different classes of objects, especially the current epoch with so many ongoing and upcoming photometric surveys.

In this work, we have used only 2MASS and WISE photometry, but the classification may be even expand to other wavelengths ranges as well.

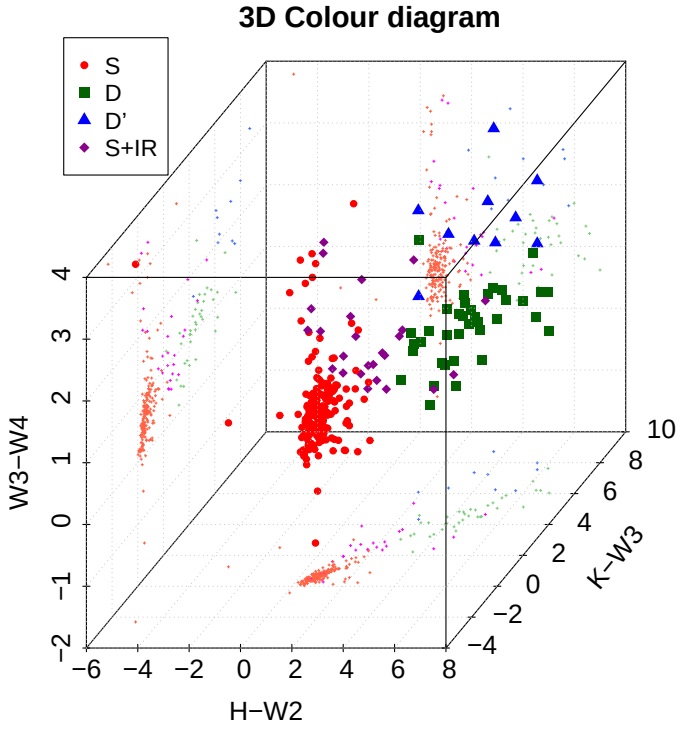

Figure 10. 3D Colour diagram of the four types of SySts. The colour indices have been obtained from the classification tree algorithm.

4 LINEAR DISCRIMINANT ANALYSIS AND K-NEAREST NEIGHBOUR METHOD

4.1 LDA

For a more robust identification/discrimination of SySts, we also explore the linear discriminant analysis (LDA) method or the Fisher discrimination analysis (Fisher 1936, Rao 1948). The main idea of this technique is to find the discriminant components, the linear correlation of a set of observed variables (such as the 2MASS and WISE photometry), which better distinguish two known groups of object (e.g. da Silva, Milone & Rocha-Pinto 2015). For this analysis the lda and predict functions in R software were used R as well as the training samples SySts/PNe/Be, SySts/CV/Mira, SySts/CV/YSO, SySts/WR/post-AGB, SySts/K-giants/M-giants, SySts/WTT/ClTT and SySts/Be/AeBe. The LDA algorithm is not applied to the training sample of SySts and mimics because of their imbalanced samples which would result to a poor classification. LDA is more depended on the sample sizes of training samples than classification tree.

First of all, we applied the LDA method to the training sample of the different types of SySts in order to examine how the different type of SySts are separated. The resulting discriminant components LD1 and LD2 that provide the best separation of the four type of SySts are given below.

$$LD1 = 1.947 + 0.314J - 0.663H - 1.426K - 0.373W1 + 1.385W2 + 0.100W3 + 0.742W4 \quad (1)$$

$$LD2 = -1.236 + 1.187J + 1.967H - 4.022K + 1.235W1 - 1.417W2 - 0.033W3 + 1.081W4 \quad (2)$$

Figure 11 displays the coefficient spectrum plot of the discriminant components. In all the plots of Table B1, the red colour corresponds to the first discriminant component (LD1) and the blue to the second component (LD2)[3]. Moreover, the so-called "proportion of trace" or discriminability of each component – the proportion of each component that explains the between-groups variance in a given data set – is given in percentage for each component. For the case of the four types of SySts, the discriminability is found 0.84 and 0.14 per cent for the to components, respectively.

4.2 KNN

In addition to the LDA algorithm, we also apply the K-nearest neighbour (KNN) method on the LDA components in order to explore the locus of each type of SySts or among the different class of sources in the training samples.

To perform this analysis, as describe below, we used the following external R packages: *class* to apply the KNN method, *dplyr* for data manipulation and *ggplot2* for graphical purpose. First, we randomly mixed our sample of 220 known Galactic SySts (with available 2MASS and AllWISE data) and selected 80% of them as training set and 20% as testing set. Secondly, the LD1 and LD2 entries were normalized (equations in Appendix B) in order to avoid different weights between the parameters. Then, we performed the KNN calculation in the training sample and used the testing sample to verify the accuracy of the results. This procedure was repeated a few times to examine how the accuracy would change when different random training/testing sample are chosen. Assuming the accuracy increases with the growth of the sample, we applied the KNN technique one last time, but now to the whole sample of 220 Galactic SySts. We find that the accuracy is in the range between 85 and 96 per cent.

In Figure 12, we present the normalised LD1 versus LD2 plot and the results obtained from the KNN analysis. The dots with a black contour represent the observed data and the background dots (with no contours) identify the regions expected for each one of the SySts types to occur. The size of the background dots is proportional to the probability of a given source of belonging to that class. We notice some clear overfitting in a few regions of the border between the different types (e.g. isolated, tiny background red dots appear around x = 0.4, y = 0.4). This occur in regions where probabilities are anyway low, and are similar for two or more types. Thus, the classification of an unknown source is uncertain on those areas. In conclusion, one should always have the probabilities in mind when studying this plot.

It is important to clarify that for the LDA and KNN analysis we conclude that the "a priori" classification of each

[3] For the cases in which CVs are used the *W3* and *W4* magnitudes were not used due to the upper limit values of CVs in these two bands.

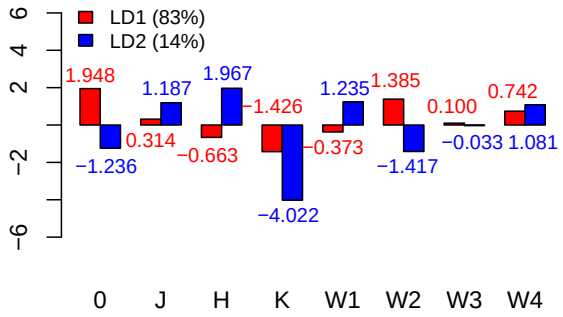

Figure 11. Coefficient spectrum plot among the four types of SySts. The "proportion of trace" or discriminability of each component is given in percentage (see text for more details). The third linear discriminant component is not presented since provides only 1% of discriminability. The "0" parameter corresponds to the zero point of the linear discriminant components due to the scaling so that the variables have mean value zero.

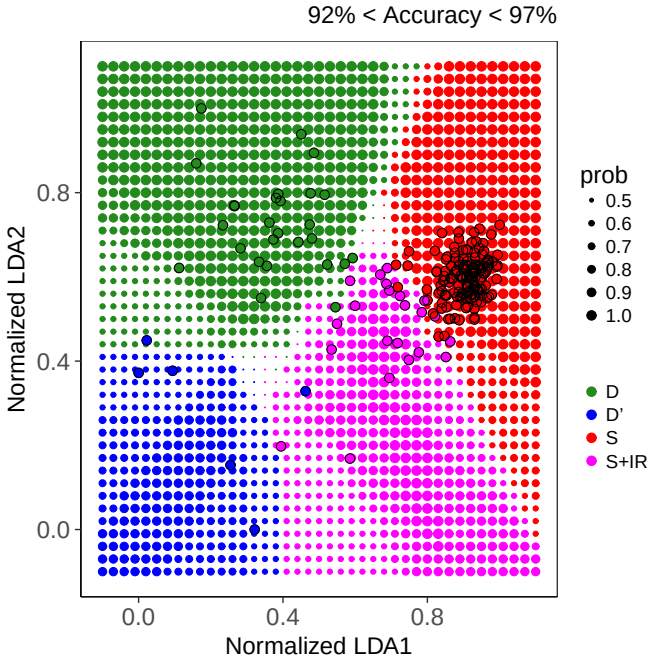

Figure 12. Plot of normalised LDA components overlaid the four regions defined by the KNN algorithm of each SySt type (LDA/KNN plot). Different colour corresponds to different type of SySts. The size of the background circles corresponds to the probability of being classified as a specific type.

Galactic SySt (taken from Paper I) is correct except from some cases. These classifications were used as input in the LDA and KNN calculations. The outliers that one can identify in Figure 12 do not imply that they are wrongly classified before, as we do expect that some mixture naturally exists between the different type clusters. Thus, as stated above, a random position in the S+IR region (magenta colour) of the plot can still has a non-zero probability to shelter D-type (green) sources for example. In conclusion, the KNN result should not be used to reclassify the objects originally used to calculate the KNN (however, it would be interesting to further investigate the nature of such outliers).

Figure 12 can be used to help classifying any newly observed source. To transform any set of 2MASS and AllWISE magnitudes into the coordinates of the figure, one should apply the relations:

$$NormalizedLD1 = \frac{(LD1 + 10.20)}{13.21} \quad (3)$$

$$NormalizedLD2 = \frac{(LD2 + 8.12)}{13.44}, \quad (4)$$

where LD1 and LD2 are given by the equations 1 and 2.

The advantage of applying KNN to the LDA components is that the locus for each type of SySts, or different class of objects can be defined with a more robust technique whereas the probabilities of being a specific type of objects are also determined.

4.3 Characterising SySts with LDA and KNN

We then applied the LDA and KNN methods to the training samples of different classes of objects – also applied to the classification tree – in order to find those models that provide the best discrimination. For several training samples, we find an LDA model that separates SySts from other stellar objects very well. The coefficients of the first (LD1) and the second (LD2) discriminant components as well as the LDA/KNN plots of the normalised LDA components are given in Table B1.

The LDA method provides a very important framework for discriminating objects. For most of the training samples examined in this work, SySts are found to fill a clearly distinguished locus. However, the discrimination is not the best for the case of the SySts/Mira/CV and SySts/CV/YSO training samples due to the limitation of not using the *W3* and *W4* magnitudes.

5 APPLICATION TO REAL DATA

Having already developed the classification criteria, the next logical step is to look for new candidate SySts in publicly available catalogues. Our classification tree criteria derived from the training sample of SySts and mimics were applied to the list of candidate SySts (Paper I, Belczyński et al. 2000), to the IPHAS list of candidate SySts (Corradi et al. 2008) and finally to the second data release of the VPHAS+ catalogue (Drew et al. 2014) in order to search for a hidden SySts population.

We found 13 strong candidate SySts in the list of candidates from Paper I, 9 new candidates in the IPHAS list

of candidates SySts (2 S-type and 7 D-type), and 63 new candidates (34 S-type and 29 D-type) in the DR2 VPHAS+ catalogue (Table **??**). The classification tree criteria were applied directly to the first two list of candidates whereas for the VPHAS+ catalogue, we should first apply the IPHAS H α excess criterion in order to get only the sample of strong H α-emitters (Corradi et al. 2008, Rodríguez-Flores et al. 2014). Additional criteria regarding the quality of the measurements (photometric errors) were also applied. In particular, we accepted as candidates only the sources with errors in the H α, r and i bands less than 0.1 (or signal to noise higher than 10) for both catalogues, IPHAS and VPHAS+. Moreover, we restricted the selection of the candidates based on their error in the 2MASS (less than 0.2) and AllWISE data (less than 0.3). The AllWISE images of the candidates were also visually inspected to ensure that a compact source is present in all the bands.

The particular case of W16-294 in the list of candidates SySts (Paper I), a sources with strong H α and He II lines as well as a red continuum spectrum of a K giant star (Mikolajewska, Acker & Stenholm 1997), satisfies all the classification tree criteria. We thus argue that it is a genuine SySts.

Certainly, there are several known, spectroscopically confirmed, SySts in the IPHAS candidate list and the VPHAS+ cataloque (column nine in Table **??**). In particularly, there are 10 known SySts in the IPHAS list and all of them were recovered (100 per cent success). By cross-matching the whole DR2 IPHAS catalogue with the list of known SySts (Paper I), we found that there are in total 27 known SySts. Many of them are not included in the IPHAS list of candidates because of no available r, i, and/or H α magnitudes. According to our classification criteria, only 18 out of 27 SySts or 66 per cent are recovered. But, 6 of them are classified as S+IR, D and D′-type and it is well known that they are not recovered with the current colour criteria (see §3, Fig. 7). This signifies that the current criteria recover 18 out of 21 known S-types SySts or 86% success.

As for the DR2 VPHAS+ catalogue, there are 40 known SySts and 27 of them are classified as S-type and 13 as S+IR, D and D′-type. We recovered 23 out of 27 known S-type or 85 per cent. Note that only 13 are presented in Table **??**. The rest of them do not pass the IPHAS criterion (not available r, i and H α magnitudes). The four missing S-type SySts that do not satisfy the classification criteria are: (i) SS73 17: J–H=0.67 with a photometric H error of 0.21 mag , (ii) Hen 3-1410: K_s–$W3$=1.29, (iii) K 6-6: K_s–$W3$=2.29 and (iv) AS 289: $W1$–$W4$=1.05. In conclusion, three of them could be recovered but they show slightly different colour indices while K 6-6 exhibits strong K_s–$W3$ excess indicative of an S+IR-type SySt.

Recall that the classification criteria derived from the SySts and mimics training samples do not recover the dusty ones (S+IR, D and D′-type, Fig. 7). Therefore, we also applied the classification criteria derived from the training samples of dusty SySts and mimics (Figure 8). These criteria revealed three more candidate SySts in the list of candidates, seven in the IPHAS list of candidates and 29 in the DR2 VPHAS+ catalogue. Regarding the known SySts in the IPHAS and VPHAS+ catalogues, there are 14 D-type, 6 S+IR-type and 1 D′-type SySts. 93 per cent of the D-type are recovered but none of the S+IR or D′-type since all S+IR have H–$W2$<3.806 and all D′type have $W1$–$W4$>4.715.

In order to verify the feasibility of our method, we also examined whether the non-SySt sources (spectroscopically classified) in Rodríguez-Flores et al. (2014) satisfy our criteria. After analysing all of the 13 sources, we found out that only one of them (IPHASJ201550.96+373004.2) satisfies all the criteria of being SySts. This candidate emerged from the dusty SySts/mimics model which suffers by a 25 per cent of contamination (see § 3). All the 13 sources were later observed and none of them was found to be a SySt. The IPHASJ201550.96+373004.2 candidate that satisfies out criteria was classified as a Be star or YSO (Rodríguez-Flores et al. 2014). This is a strong proof that our classification criteria works very well, and it can indicate very likely SySts candidates or reject sources from follow-up observations.

Corradi et al. (2010) have also obtained spectroscopic data of two sources in our list of candidate SySts (IPHASJ194907.23+211742.0 and IPHASJ202947.93+355926.5). The first one is a young PN but according to Viironen et al. (2009) its spectrum resembles those of D-type SySts and it may belong to the rare group of objects whose its nature is still not clear like M 2-9. The second one is classified as YSO (see also Krause et al. 2003). Our classification criteria also indicate a likely YSO or AeBe star. Note that the last two objects were derived from the dusty/mimic model for which the group of SySts suffers by a 25 per cent contamination. Therefore, the possibility of finding other dusty sources like YSO is not small.

Baella et al. (2016) also searched for new yellow SySts by observing five candidate SySts and they ended up discovering one new SySt (StHa 63) while the remaining sources were classified as K giants. From our classification criteria, we conclude that all of them are good candidate SySts and deserved to be observed. Nevertheless, by using the criteria from the SySts+K/M giants training sample (Fig. A5), only two objects StHa 63 (the confirmed) and SS 360 (classified as M3 III, see Baella et al. 2016) pass the criteria of being SySts while the remaining not.

The interesting point here is that SySts with low luminosity WDs produce very weak optical emission line and they can be misclassified. SU Lyn belongs to this specific group of SySts. Despite its optical spectrum resembling that of an M6 III star having a very weak H α emission line, its UV-excess indicates the presence of a hot white dwarf (Mukai et al. 2016). According to our classification tree criteria, SU Lyn is indeed a SySt and not an isolate red giant. Therefore, we claim that SS 360 may also be a member of SySts with a low luminosity WD. Notice that SS 360 is the only object, besides StHa 63, with an H α emission (see Fig. 4 in Baella et al. 2016).

The final step is to apply our classification tree and LDA/KNN criteria derived from the training samples of different classes of sources to our list of candidate SySts. In Tables **??** and **??**, we present a probable classification of each source in columns 2 to 8, for the classification tree and LDA/KNN methods, respectively. All the known SySts in this list are recovered from both methods. Therefore, at least an 80-90 per cent of the sources are very likely SySts. A spectroscopic study of these sources will be presented in a forthcoming paper.

6 DISCUSSION AND CONCLUSIONS

We carried out and presented a machine learning approach to find new SySts in publicly available H α photometric catalogues using H α-excess, 2MASS and WISE photometric data. First, we explored a number of different combinations of colour indices that can provide a good separation of SySts from other classes of objects that mimic SySts such as PNe, post-AGB stars, CVs, WR stars, WTT and ClTT stars, single K and M giants, and Be stars. We shown that the widely used *J–H* vs. H–K_s is not an adequate DCCD for identifying SySts. S-type SySts, Mira, YSO and WTT stars occupy the same regions making very hard to distinguish them. The *W3–W4* vs. K_s–*W3* and *J–H* vs. *W1–W4* DCCDs were found to be better DCCDs.

Machine learning methods such as classification tree, linear discriminant analysis and K-nearest neighbours were also used to derive new criteria that distinguish SySts from other stellar objects. Classification tree revealed that the K_s–*W3*, *H–W2* and *W3–W4* colour indices are the best observable parameters for classifying SySts into the S, D, D′and S+IR scheme. The *J–H*, K_s–*W3*,*W1–W2* colour indices were found to provide the best combination for separating S-type SySts from mimics, whereas the *H–W2* and *W1–W4* colour indices are better for identifying the dusty SySts. By training the classification tree using samples with different combinations of classes of objects, we deduced that primarily *J–H*, *W1–W4* and K_s–*W3* and secondarily *H–W2*, *W1–W2* and *W3–W4* provide ideal colour indices to distinguish SySts.

Linear discrimination analysis and K-nearest neighbour were also used in order to find the linear combination of 2MASS and AllWISE data, that better discriminate SySts. SySts were found to define, in most of the cases, distinct regions. Diagnostic diagrams obtained from the LDA+KNN analysis were also provided. The accuracy of these diagrams vary between 80 and 98 per cent. Mira stars were found to be the objects which cannot be easily distinguished from the SySts, especially the S-type, as they have very similar colour indices.

Finally, we applied our classification tree model derived from the SySts and mimics training samples to the list of candidate SySts from Paper I, the IPHAS list of candidate SySts, and the DR2 VPHAS+ catalogues. We ended up with 125 sources that pass the criteria. 72 of them (36 S-type and 36 D-type) are new candidate SySts. All the criteria derived from the training samples with different combinations of sources were also applied to our final list of candidates and the most likely identification was provided for each source. Our models recovered up to 90 per cent of the known SySts in these three lists. Around 80-90 per cent of the sources in our list are very likely SySts but a spectroscopic confirmation is required.

ACKNOWLEDGMENTS

All the authors thank the anonymous referee for very insightful comments and for helping us to significantly improve our paper. S.A. and M.L.L.-F. acknowledge support of CNPq, Conselho Nacional de Desenvolvimento Científico e Tecnológico - Brazil (grant 300336/2016-0 and 248503/2013-8 respectively). GRL acknowledges support from Universidad de Guadalajara, CONACyT, PRODEP and SEP (Mexico). LGR is supported by NWO funding towards the Allegro group at Leiden University. Authors would like to thank Vaselina Kalinova, Dario Colombo, Jens Kauffmann and Helio Jaques Rocha-Pinto for the fruitful discussion on machine learning. M.L.L.-F. would also like to thank Xander Tielens and Richard Stancliffe, for host him in their respective research groups at the Leiden Observatory and Argelander Institüt fur Astronomie. This publication makes use of data from the Two Micron All-Sky Survey which is a joint project of the University of Massachusetts and the Infrared Processing and Analysis Center/California Institute of Technology, funded by the NASA and the National Science Foundation, data products from the Wide-field Infrared Survey Explorer, which is a joint project of the University of California, Los Angeles, and the Jet Propulsion Laboratory/California Institute of Technology, funded by the National Aeronautics and Space Administration. This paper also makes use of data obtained as part of the INT Photometric H α Survey of the Northern Galactic Plane (IPHAS, www.iphas.org) carried out at the Isaac Newton Telescope (INT). The INT is operated on the island of La Palma by the Isaac Newton Group in the Spanish Observatorio del Roque de los Muchachos of the Instituto de Astrofisica de Canarias. All IPHAS data are processed by the Cambridge Astronomical Survey Unit, at the Institute of Astronomy in Cambridge. The band merged DR2 catalogue was assembled at the Centre for Astrophysics Research, University of Hertfordshire, supported by STFC grant ST/J001333/1. Based on data products from observations made with ESO Telescopes at the La Silla Paranal Observatory under programme ID 177.D-3023, as part of the VST Photometric H α Survey of the Southern Galactic Plane and Bulge (VPHAS+, www.vphas.eu). Finally, this publication makes use of many software packages in Python, including: Matplotlib (Hunter 2007), NumPy (van der Walt et al. 2011), SciPy (Jones et al. 2001) and AstroPy Python (Astropy Collaboration et al. 2013; Muna et al. 2016).

REFERENCES

Akras S., Ramírez Vélez J. C., Nanouris N., Ramos-Larios G., López J. M., Hiriart D., Panoglou D., 2017, MNRAS, 466, 2948
Akras S., Leal-Ferreira M. L., Guzman-Ramirez L., Ramos-Larios G., 2019, Accepted to ApJ Supplements (Paper I)
Allen D. A., Glass I. S., 1974, MNRAS, 167, 337
Astropy Collaboration, Robitaille, T. P., Tollerud, E. J., et al., 2013, A&A, 558, A33
Baella N. O., Pereira C. B, Miranda L. F., 2013, AJ, 146, 115
Baella N. O., Pereira C. B., Miranda L. F., Alvarez-Candal A., 2016, AJ, 151, 100
Belczyński K., Mikolajewska J., Munari U., et al., 2000, A&AS, 146, 407
Benitez N., et al., 2014, arXiv1403.5237
Buntine W., Chapman & Hall, London, 1993, in Hand D. J., ed., Learning classification trees. Artificial Intelligence frontiers in statistics. p. 182
Carlberg J. K., Majewski S. R., Patterson R. J., Bizyaev D., Smith V. V., Cunha K., 2011, ApJ, 732, 39
Catchpole R. M., Glass I. S., 1974, MNRAS, 169, 69,
Cenarro A. J., et al., 2018, A&A, in press, preprint (arXiv:1804.02667)

Chojnowski S. D., et al., 2015, AJ, 149, 7
Cieza L., et al., 2007, ApJ, 667, 308
Clyne N., Akras S., Steffen W., Redman M. P., Gonçalves D. R., Harvey E, 2015, A&A, 582, 60
Corradi R. L. M., Rodríguez–Flores E. R., Mampaso A., et al., 2008, A&A, 480, 409–419
Corradi R. L. M., et al. 2010, A&A, 509, A41
Cutri R. M., et al., 2003, VizieR Online Data Catalog, 2246
Cutri R. M., et al., 2014, VizieR Online Data Catalog, 2328
Da Silva R., Milone A. d. C., Rocha-Pinto H. J., 2015, A&A, 580, A24
Debes J. H., Hoard D. W., Wachter S., Leisawitz D. T., Cohen M., 2011, ApJS, 197, 38D
Dilday B., Howell D. A., Cenko S. B., et al., 2012, Sci, 337, 942
Di Stefano R., 2010, ApJ, 719, 474
Drew J. E., Greimel R., Irwin M. J., Aungwerojwit A., Barlow M. J., et al., 2005, MNRAS, 362, 753
Drew J. E., Gonzalez-Solares E., Greimel R., Irwin M. J., Küpcü Yoldas A., et al., 2014, MNRAS, 440, 2036D
France K., Schindhelm E., Bergin E. A., Roueff E., Abgrall H., 2014, ApJ, 784, 127
Fisher R. A., 1936, Annals of Eugenics, 7, 179
Galli P. A. B., Bertout C., Teixeira R., Ducourant C., 2015, A&A, 580, 26
Greiss S., et al., 2012, AJ, 144, 24
Gromadzki M., Mikolajewska J., Whitelock P., Marang F., 2009, AcA, 59, 169G
Grubinger T., Zeileis A., Pfeiffer K.-P., 2011, Journal of statistical software, 61
Gutiérrez-Moreno A., Moreno H., Cortés G., 1995, PASP, 107, 462
Gray R. O., et al., 2016, AJ, 151, 13.
Grankin K. N., Melnikov S. Y., Bouvier J., Herbst W., Shevchenko V. S., 2007, A&A, 461, 183
Grankin K. N., Bouvier J., Herbst W., Melnikov S. Y., 2008, A&A, 479, 827
Han Z., Podsiadlowski Ph., 2004, MNRAS, 350, 1301
Harvey P., Merín B., Huard T. L., Rebull L. M., Chapman N., Evans N. J. II, Myers P. C., 2007, ApJ, 663, 1149
He H., Garcia E. A., 2009, IEEE Trans. Knowledge and Data Engineering, 21, 1263
Herbst W., Shevchenko V. S., 1999, AJ, 118, 1043
Hoard D. W., Wachter S., Clark L. L., Bowers T. P., 2002, ApJ, 565, 511
Huemmerich S., Bernhard K., 2012, Open European Journal on Variable Stars, 149, 1
Hunter J. D., 2007, CSE, 9, 90
Ilkiewicz K., Mikolajewska J., 2017, A&A, 606, 110
Ivison R. J., Seaquist E. R., Schwarz H. E., Hughes D. H., Bode M. F., 1995, MNRAS, 273, 517I
Jones E., Oliphant T., Peterson P., et al., 2001, SciPy:Open source scientific tool for Python, http://www.scipy.org/.
Jordan S., Schmutz W., Wolff B., Werner K., Muerset U., 1996, A&A, 312, 897
Kenyon S. J., 1986, The Symbiotic Stars, Cambridge University Press, Cambridge
Kohoutek L., Wehmeyer R., 2003, AN, 324, 437K
Krause et al. 2003, A&A, 398, 1007
Leedjärv L., 1992, BaltA, 1, 59
Leedjärv L., 2004, BaltA, 13, 109
Longadge R., Dongre S., Malik L., 2013, IJCSN, 2, 83.
Lü G., Yungelson L., Han Z., 2006, MNRAS, 372 1389
Luud L., Tuvikene T., 1987, Afz, 26, 457
Luna G. J. M., Sokoloski J. L., Mukai K., Nelson T., 2013, A&A, 559, 6
Magrini L., Corradi R. L. M., Munari U., 2003, in Corradi R. L. M., Mikolajewska J., Mahoney T. J., eds, Astronomical Society of the Pacific Conference Series, Vol. 303, Symbiotic Stars Probing Stellar Evolution, p. 539 (arXiv:astro-ph/0208085)
Mikolajewska J., Acker A., Stenholm, B. 1997, A&A, 327, 191
Mikolajewska J., 2012, BaltA, 21, 5M
Mikolajewska J., Shara M. M., Caldwell N., Ilkiewicz K., Zurek D., 2017, MNRAS, 465, 1699
Miszalski B., Napiwotzki R., Cioni M.-R. L., Groenewegen M. A. T., Oliveira J. M., Udalski A., 2011, A&A, 531, A157
Miszalski B., Mikolajewska J., Udalski A., 2013, MNRAS, 432, 3186M
Moret B. M. E., 1982, Decision Trees and Diagrams,Computing Surveys (CSUR), 14, 593-623
Mukai K., Luna G. J. M., Cusumano G., Segreto A., Munari U., Sokoloski J. L., Lucy A. B., Nelson T., Nuñez N. E., 2016, MNRAS, 461, 1.
Muna, D., Alexander, M., Allen, A., et al. 2016, preprint (arXiv:1610.03159)
Munari U., Renzini A., 1992, AJ, 397, 87
Munari U., Patat F., 1993, A&A, 277, 195M
Phillips J. P., 2007, MNRAS, 376, 1120
Pereira C. B., Smith V. V., Cunha K., 2005, A&A, 429, 993P
R Development Core Team (2008). R: A language and environment for statistical computing. R Foundation for Statistical Computing, Vienna, Austria. ISBN 3-900051-07-0, URL http://www.R-project.org.
Ramos-Larios G., Phillips J. P., 2005, MNRAS, 357, 732
Rao C. R., 1948, Journal of the Royal Statistic Society, Series B (Methodological), 10, 159-203
Reid W. A., 2014, MNRAS, 438, 2642
Rebull L. M., et al., 2011, ApJS, 196, 4
Rodrigues C. V., Sartori, M. J., Gregorio-Hetem J., Magalhães A. M., 2009, ApJ, 698, 2031
Rodríguez-Flores E. R., 2006, DEA Thesis, University of La Laguna, Tenerife, Spain
Rodríguez-Flores E. R., Corradi R. L. M., Mampaso A., García-Alvarez D., Munari U., Greimel R., Rubio-Díez M. M., Santander-García M., 2014, A&A, 567, 49R
Scaringi S., Groot P. J., Verbeek K., Greiss S., Knigge C., K ording E., 2013, MNRAS, 428, 2207S
Schmeja S., Kimeswenger S., 2001, A&A, 377, 18S
Schwarz H. E., Corradi R. L. M., 1992, A&A, 265, 37S
Skopal A., Cariková Z., 2015, A&A, 573,8
Skrutskie M. F., Cutri R. M., Stiening R., et al. 2006, AJ, 131, 1163 2MASS
Suárez O., García-Lario P., Manchado A., Manteiga M., Ulla A., Pottasch S. R., 2006, A&A, 458, 173
Sokoloski J. L., 2003, JAVSO, 31, 89
Tabur V., Bedding T. R., Kiss L. L., Moon T. T., Szeidl B., Kjeldsen H., 2009, MNRAS,400,1945
Totov T., 2003, ASPC, 303, 376
van der Hucht K. A., 2001, NewAR, 45, 135
van der Walt S., Colbert S. C., Varoquaux G., 2011, ICSE, 13, 22
Venables W. N., Ripley B. D., 2002, Modern Applied Statistics with S. Fourth Edition. Springer, New York. ISBN 0-387-95457-0
Vickers S. B., Frew D. J., Parker Q. A., Bojičić I. S., 2015, MNRAS, 447, 1673
Vieira S. L. A., Corradi W. J. B., Alencar S. H. P., Mendes L. T. S., Torres C. A. O., Quast G. R., Guimarães M. M., da Silva L., 2003, AJ, 126, 2971
Viironen K., Greimel R., Corradi R. L. M., et al., 2009, A&A, 504, 291
Visa S., Ralescu A., in Proceedings of the Sixteen Midwest Artificial Intelligence and Cognitive Science Conference, 2005, 67-73.
Yoon D.-H., Cho S.-H., Kim J., Y. Y. j., Park Y.-S., 2014, ApJS, 211, 15
Wang B., Liu Z., Han Y., Lei Z., Luo Y., Han Z., 2010, ScChG, 53, 586

Weiss G. M., Provost F., 2003, Journal of Artificial Intelligence Research, 19, 315
Whitelock P. A., Feast M. W., Van Leeuwen F., 2008, MNRAS, 386, 313
Wickham, H. 2009, ggplot2: Elegant Graphics for Data Analysis. Springer-Verlag New York
Wickham H., Francois R., 2016, dplyr: A Grammar of Data Manipulation. R package version 0.5.0. https://CRAN.R-project.org/package=dplyr
Witham, A.R., Knigge, C., G ÌĺLansicke, B.T., Aungwerojwit, A., et al., 2006, MNRAS 369, 581
Wright E. L., Eisenhardt P. R. M., Mainzer A. K., et al., 2010, AJ, 140, 1868
Zamanov R. K., Bode M. F., Melo C. H. F., Porter J., Gomboc A., Konstantinova-Antova R., 2006, MNRAS, 365, 1215
Zamanov R. K., Bode M. F., Melo C. H. F., Stateva I. K., Bachev R., Gomboc A., Konstantinova-Antova R., Stoyanov K. A., 2008, MNRAS, 390, 377

APPENDIX A: CLASSIFICATION TREE

The classification tree plots derived from the training samples of the following groups: SySts/PNe/Be, SySts/CV/Mira, SySts/CV/YSO, SySts/WR/post-AGB, SySts/K-giants/M-giants, SySts/WTT/ClTT and SySts/Be/AeBe are presented here.

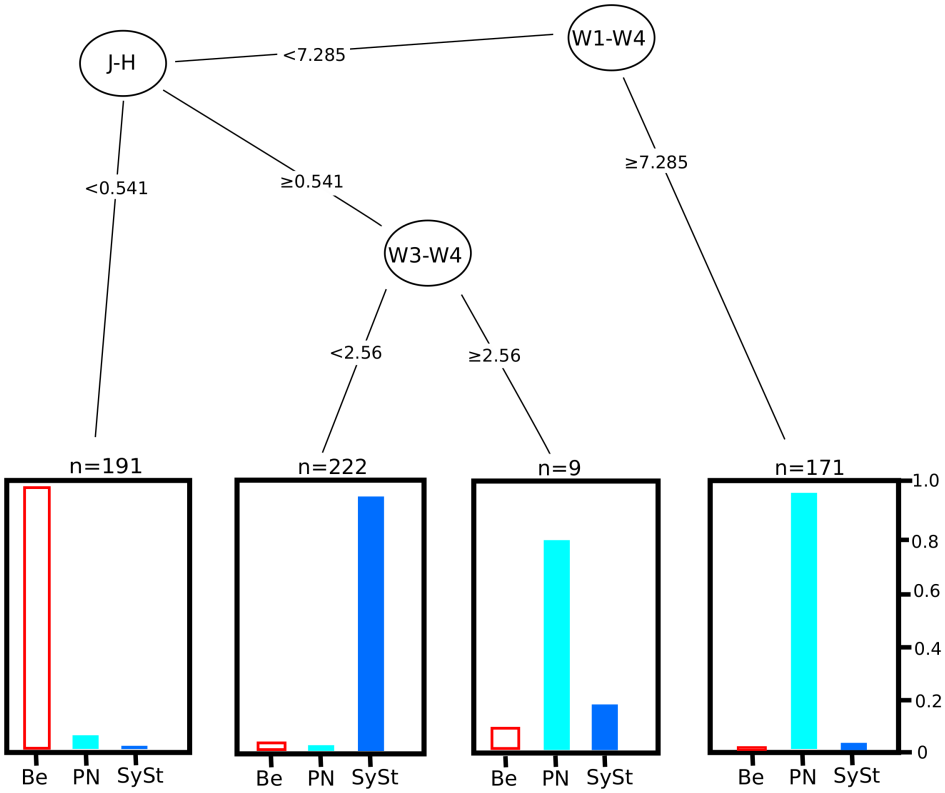

Figure A1. Classification tree plot from the SySts/PNe/Be training sample.

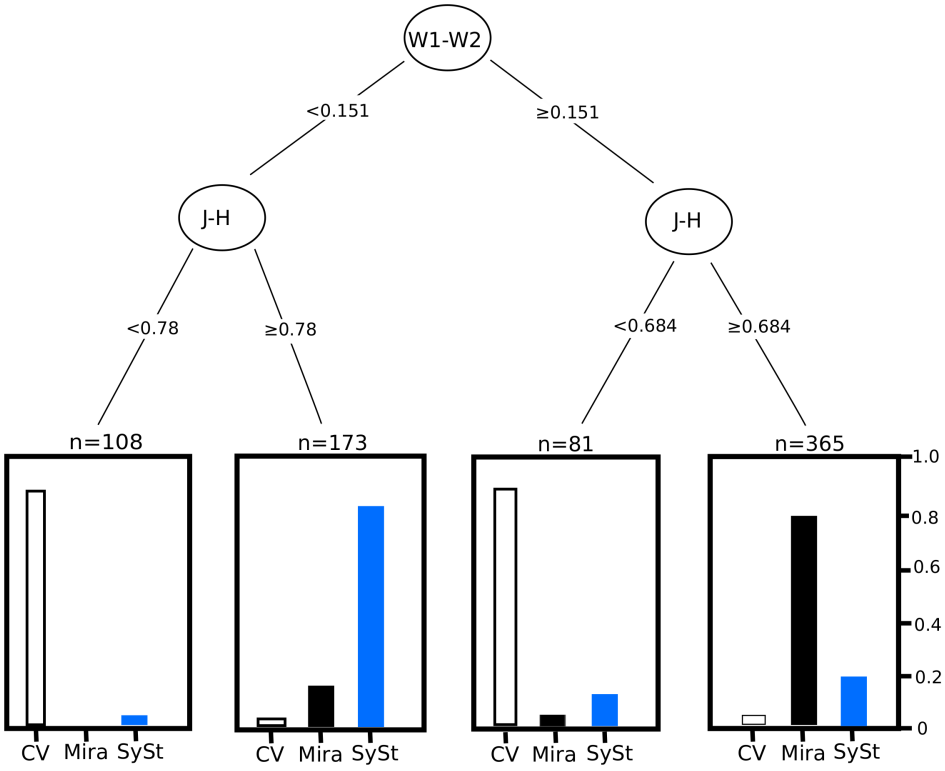

Figure A2. Classification tree plot from the SySts/CV/Mira training samples.

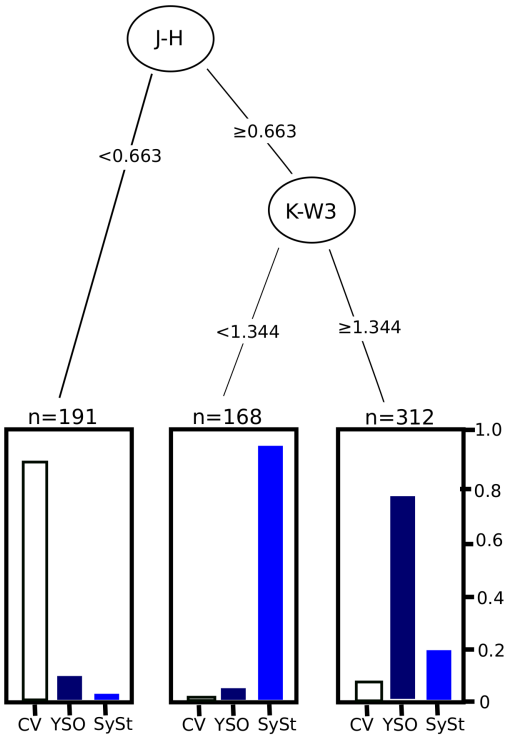

Figure A3. Classification tree plot from the SySts/CV/YSO training sample.

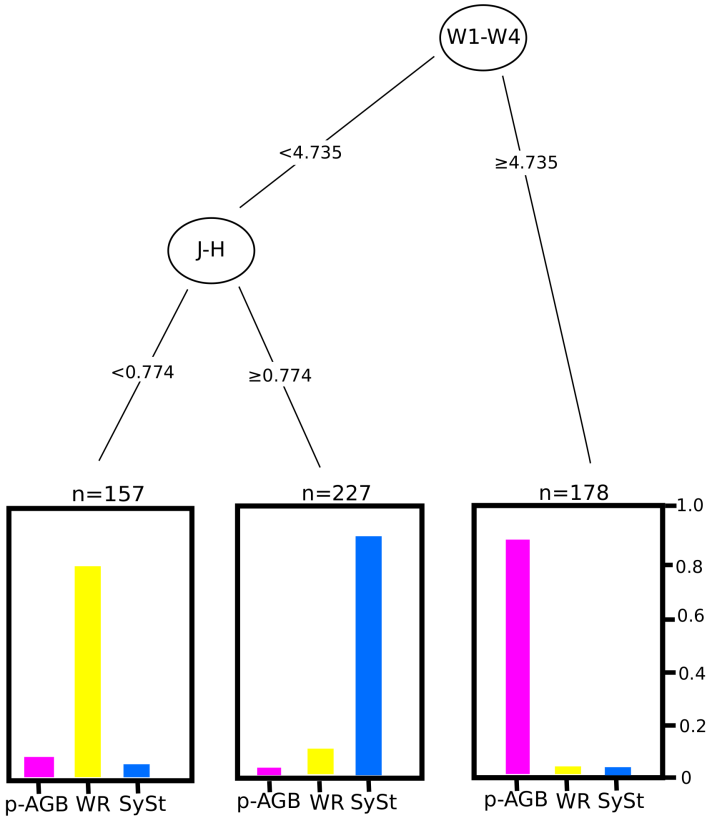

Figure A4. Classification tree plot from the SySts/WR/post-AGB training sample.

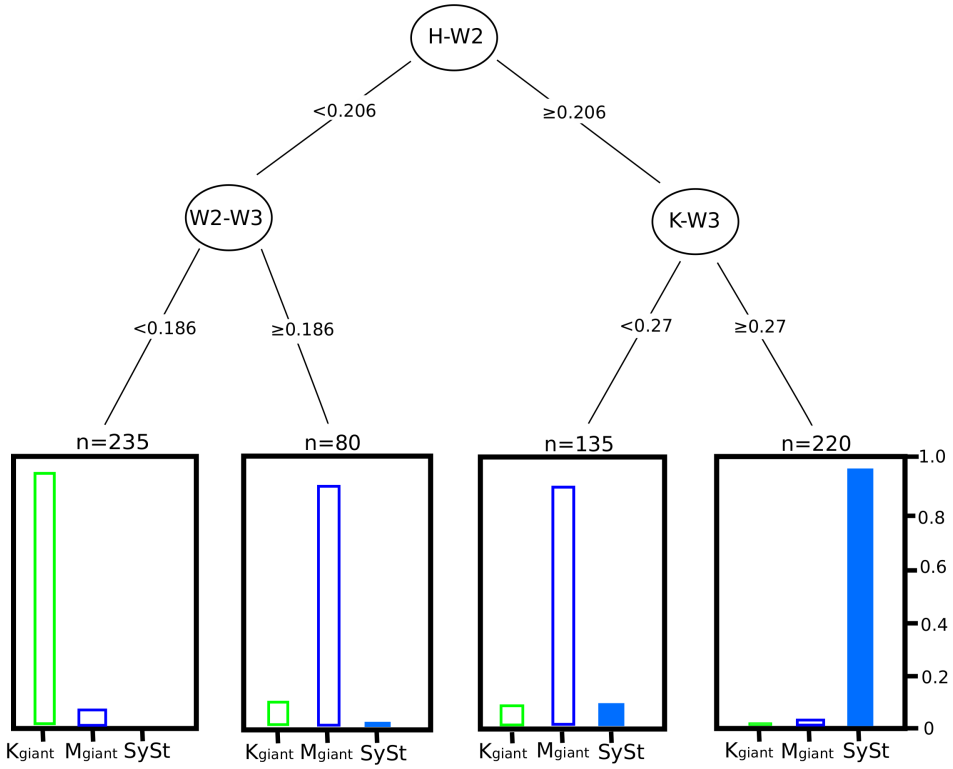

Figure A5. Classification tree plot from the SySts/K-giants/M-giants training sample.

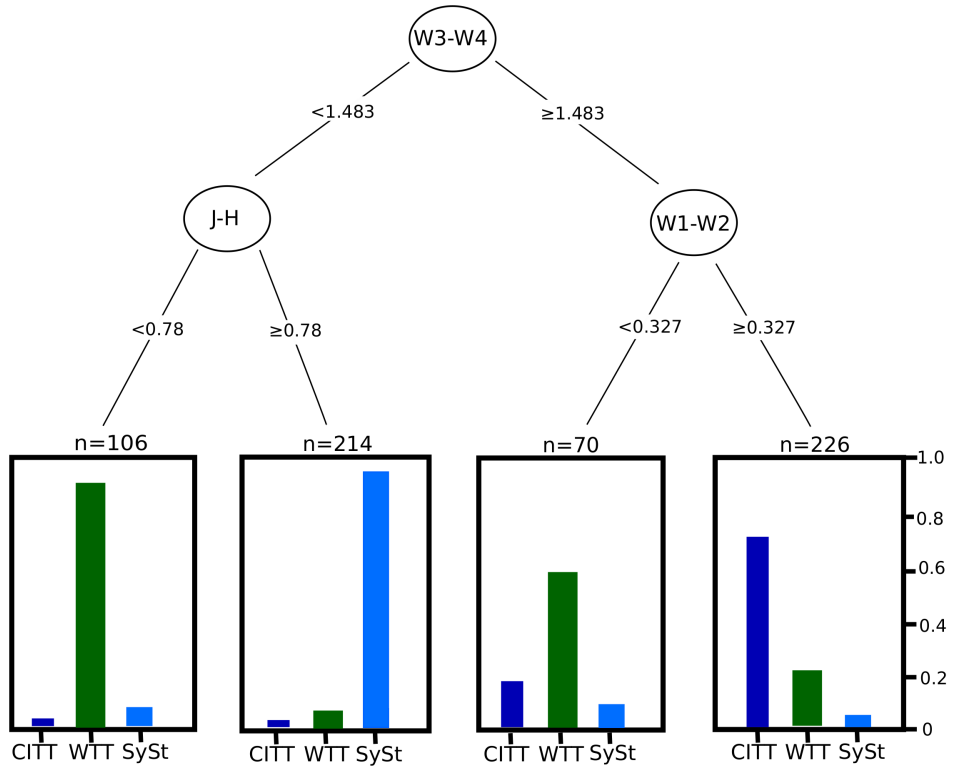

Figure A6. Classification tree plot from the SySts/WTT/ClTT training sample.

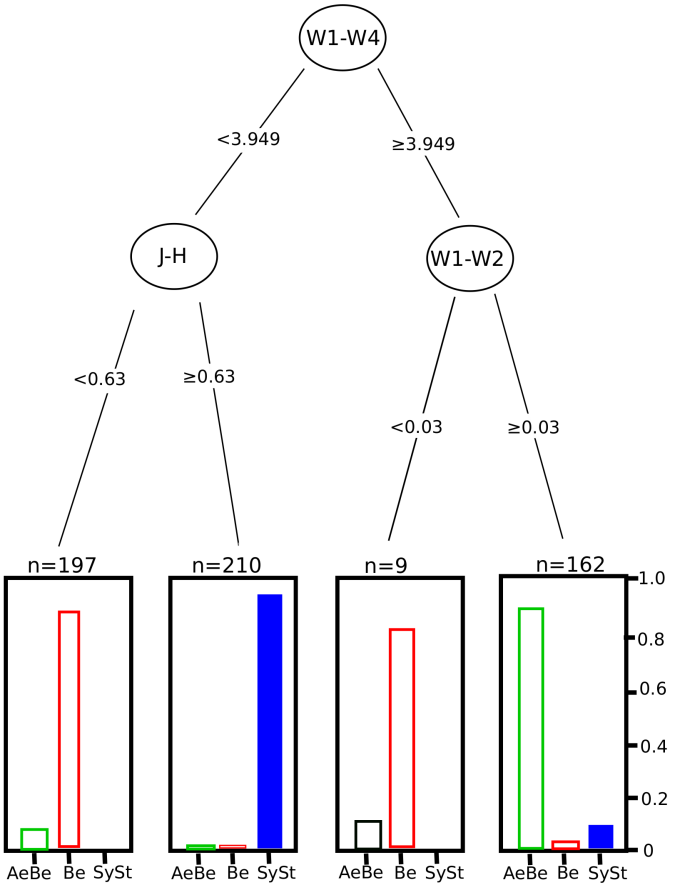

Figure A7. Classification tree plot from the SySts/Be/AeBe training sample.

APPENDIX B: LDA+KNN

To transform any set of linear discriminant components (LD1 and LD2) obtained from the coefficients in Table B1 into the range [0,1] one should apply the following relations:

- Data set: SySts - PNe - Be

$$NormalizedLD1 = \frac{(LD1 + 5.65)}{9.28} \quad \text{(B1)}$$

$$NormalizedLD2 = \frac{(LD2 + 8.38)}{11.67}, \quad \text{(B2)}$$

- Data set: SySts - CV - Mira

$$NormalizedLD1 = \frac{(LD1 + 6.35)}{12.19} \quad \text{(B3)}$$

$$NormalizedLD2 = \frac{(LD2 + 3.40)}{8.47}, \quad \text{(B4)}$$

- Data set: SySts - YSO - CV

$$NormalizedLD1 = \frac{(LD1 + 4.46)}{9.06} \quad \text{(B5)}$$

$$NormalizedLD2 = \frac{(LD2 + 3.36)}{8.86}, \quad \text{(B6)}$$

- Data set: SySts - post-AGB - WR

$$NormalizedLD1 = \frac{(LD1 + 4.87)}{7.49} \quad \text{(B7)}$$

$$NormalizedLD2 = \frac{(LD2 + 7.28)}{10.50}, \quad \text{(B8)}$$

- Data set: SySts - M giants - K giants

$$NormalizedLD1 = \frac{(LD1 + 2.21)}{11.87} \quad \text{(B9)}$$

$$NormalizedLD2 = \frac{(LD2 + 4.81)}{10.81}, \quad \text{(B10)}$$

- Data set: SySts - WTT - ClTT

$$NormalizedLD1 = \frac{(LD1 + 4.77)}{11.53} \quad \text{(B11)}$$

$$NormalizedLD2 = \frac{(LD2 + 4.47)}{6.69}, \quad \text{(B12)}$$

- Data set: SySts - Be - AeBe

$$NormalizedLD1 = \frac{(LD1 + 4.89)}{13.16} \quad \text{(B13)}$$

$$NormalizedLD2 = \frac{(LD2 + 2.69)}{7.77}, \quad \text{(B14)}$$

The LDA/KNN plots derived from the training samples of the following groups: SySts/PNe/Be, SySts/CV/Mira, SySts/CV/YSO, SySts/WR/post-AGB, SySts/K-giants/M-giants, SySts/WTT/ClTT and SySts/Be/AeBe are presented here.

APPENDIX C: VERY LIKELY CANDIDATE SYSTS IN IPHAS AND VPHAS+ CATALOGUES

The list of 125 sources found in the list of the candidate SySts (paper I), the IPHAS list of candidate SySts (Corradi et al. 2008) and the DR2 VPHAS+ catalogue (Drew et al. 2014) are presented here. The classification of each source based on the classification tree and LD/KNN is also provided in the columns 2 to 8 as follows: (a) SySts/PNe/Be, (b) SySts/CV/Mira, (c) SySts/CV/YSO, (d) SySts/WR/post-AGB, (e) SySts/K-giants/M-giants, (f) SySts/WTT/ClTT, (g) SySts/Be/AeBe.

Table B1. LDA & KNN modelling

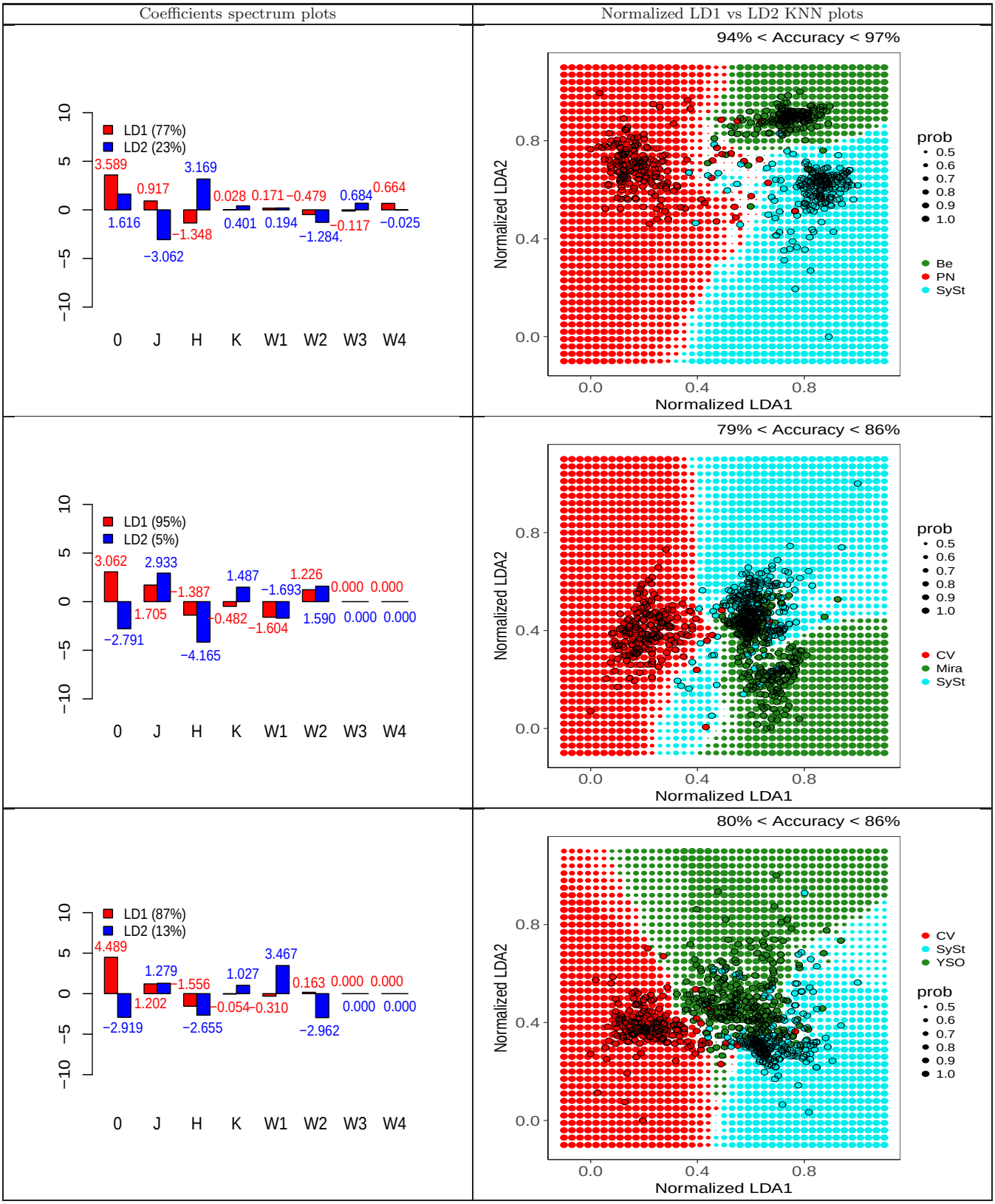

Left column: Coefficient spectrum plot of the first (red) and second (blue) discriminant components for the seven-dimensional space of 2MASS and WISE surveys. "0" variable corresponds to the zero point. The numbers in parenthesis give the percentage of discriminabily. Right column: The LDA/KNN plots for different sets of objects. The size of the background circles corresponds to the probability of being classified as a specific type. The equations to normalize the LDA components and produce the KNN plots are given in Appendix A.

Table B1. LDA & KNN modelling

Coefficients spectrum plots	Normalized LD1 vs LD2 KNN plots
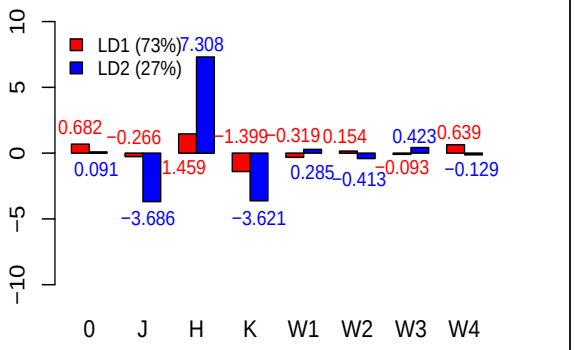	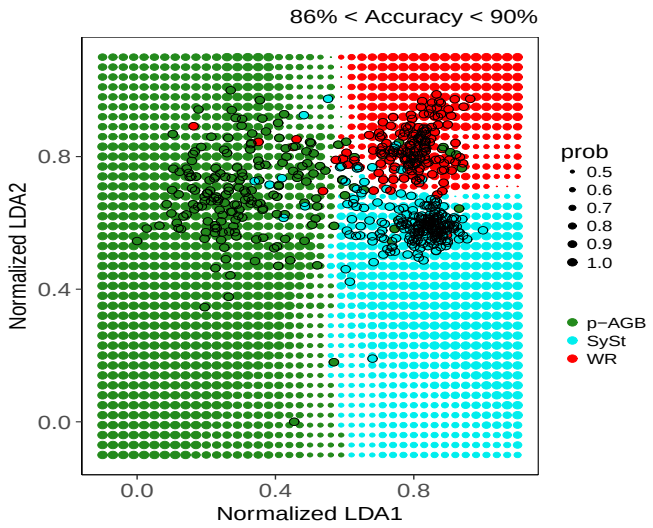
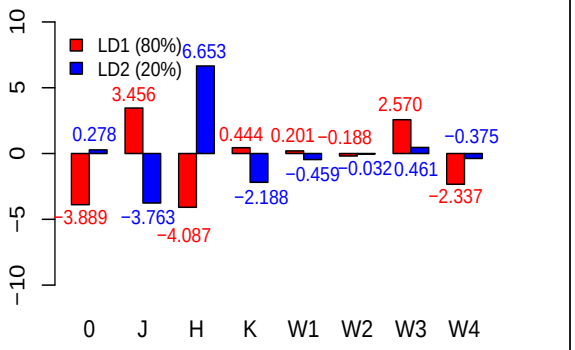	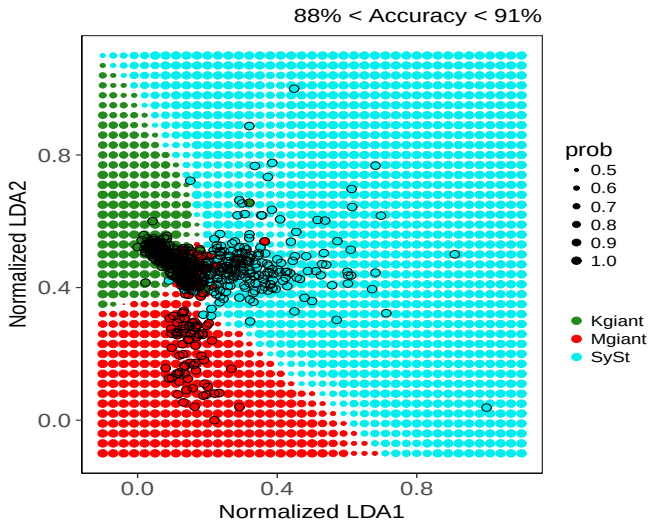
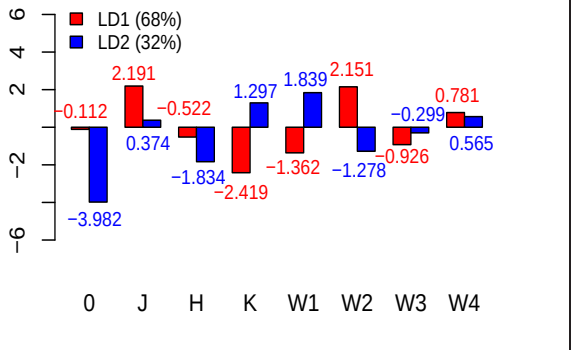	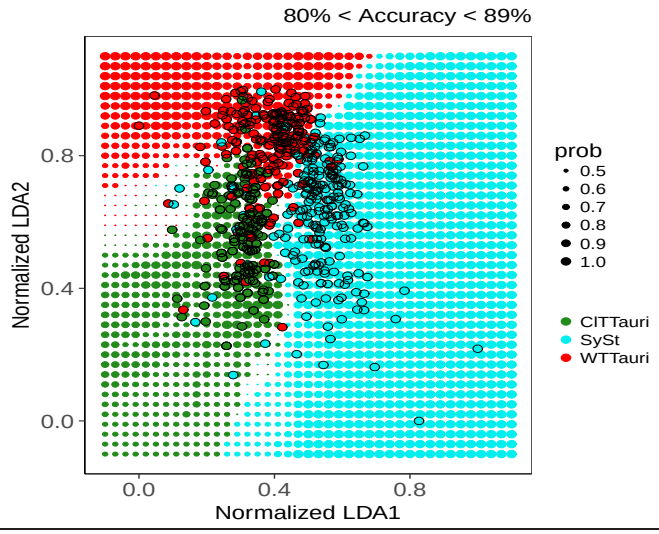

Left column: Coefficient spectrum plot of the first (red) and second (blue) discriminant components for the seven-dimensional space of 2MASS and WISE surveys. "0" variable corresponds to the zero point. The numbers in parenthesis give the percentage of discriminabily. Right column: The LDA/KNN plots for different sets of objects. The size of the background circles corresponds to the probability of being classified as a specific type. The equations to normalize the LDA components and produce the KNN plots are given above.

Table B1. LDA & KNN modelling

Coefficients spectrum plots	Normalized LD1 vs LD2 KNN plots
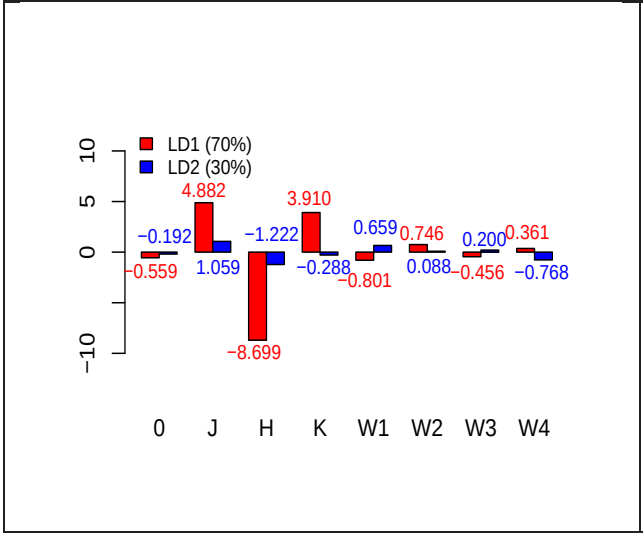	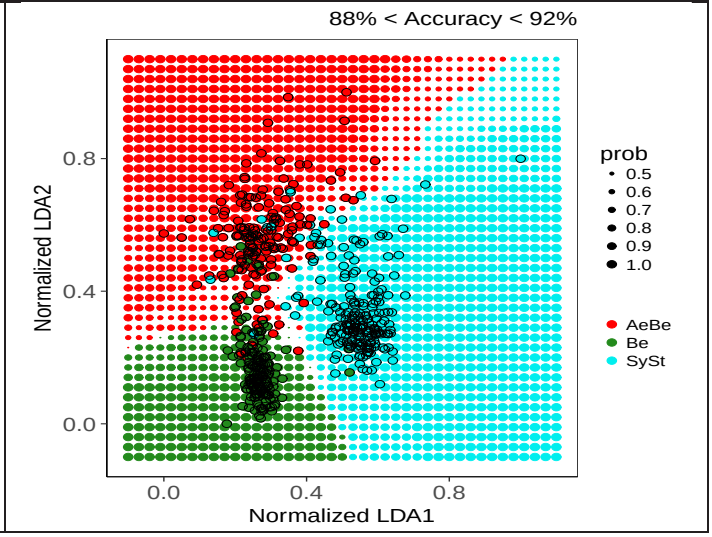

Left column: Coefficient spectrum plot of the first (red) and second (blue) discriminant components for the seven-dimensional space of 2MASS and WISE surveys. ”0” variable corresponds to the zero point. The numbers in parenthesis give the percentage of discriminabily. Right column: The LDA/KNN plots for different sets of objects. The size of the background circles corresponds to the probability of being classified as a specific type. The equations to normalize the LDA components and produce the KNN plots are given in Appendix A.

Table C1: New very likely symbiotic stars found in Paper I and the IPHAS and VPHAS+ surveys. A further classification of the candidates based on the classification tree analysis is given in columns 2 to 8: (a) SySts/PNe/Be, (b) SySts/CV/Mira, (c) SySts/CV/YSO, (d) SySts/WR/post-AGB, (e) SySts/K-giants/M-giants, (f) SySts/WTT/ClTT, (g) SySts/Be/AeBe.

Name	(a)	(b)	(c)	(d)	(e)	(f)	(g)	Comments
Candidates – Paper I								
Hen 3-653	SySt	SySt	SySt	SySt	SySt	SySt	SySt	
Hen 4-134	SySt	SySt	SySt	SySt	SySt	SySt	SySt	
Hen 4-137	SySt	SySt	SySt	SySt	SySt	SySt	SySt	
V748 Cen	SySt	SySt	SySt	SySt	SySt	SySt	SySt	
WRAY 16-294	SySt	SySt	SySt	SySt	SySt	SySt	SySt	
001.97+02.41	SySt	SySt	SySt	SySt	SySt	SySt	SySt	
001.33+01.07	SySt	SySt	SySt	SySt	SySt	SySt	SySt	
001.71+01.14	SySt	SySt	SySt	SySt	SySt	SySt	SySt	
DASCH J075731.1+201735	SySt	SySt	SySt	SySt	Mgiant	SySt	SySt	
ASAS J174600-2321.3	SySt	SySt	SySt	SySt	SySt	SySt	SySt	
dusty								
2MASSJ17145509-393311712	SySt	Mira	YSO	SySt	SySt	SySt	AeBe	
357.12+01.66	SySt	Mira	YSO	SySt	SySt	ClTTauri	AeBe	
AS 288	SySt	Mira	YSO	SySt	SySt	SySt	AeBe	
IPHAS								
stellar								
IPHASJ182906.08-003457.2	SySt	SySt	SySt	SySt	SySt	SySt	SySt	known SySt
IPHASJ183501.83+014656.0	SySt	SySt	SySt	SySt	SySt	SySt	SySt	known SySt
DQ Ser	SySt	SySt	SySt	SySt	SySt	SySt	SySt	known SySt
IPHASJ184446.08+060703.5	SySt	SySt	SySt	SySt	SySt	SySt	SySt	known SySt
IPHASJ184733.03+032554.3	SySt	SySt	SySt	SySt	SySt	SySt	SySt	known SySt
IPHASJ185039.20+065916.7	SySt	SySt	SySt	SySt	SySt	WTTauri	SySt	
IPHASJ185323.58+084955.0	SySt	SySt	SySt	SySt	SySt	SySt	SySt	known SySt
IPHASJ190924.64-010910.2	SySt	SySt	SySt	SySt	SySt	SySt	SySt	known SySt
Ap 3-1	SySt	SySt	SySt	SySt	SySt	SySt	SySt	known SySt
IPHASJ193436.06+163128.9	SySt	SySt	SySt	SySt	SySt	SySt	SySt	known SySt
IPHASJ193501.31+135427.5	SySt	SySt	SySt	SySt	SySt	SySt	SySt	known SySt
IPHASJ194120.77+245612.9	SySt	SySt	SySt	SySt	SySt	SySt	SySt	
dusty								
IPHASJ192257.72+113854.8	SySt	Mira	YSO	SySt	SySt	ClTTauri	AeBe	
IPHASJ194907.23+211742.0	SySt	Mira	YSO	SySt	SySt	SySt	AeBe	young PN (3)
IPHASJ195712.42+301316.1	SySt	Mira	YSO	SySt	SySt	SySt	AeBe	young PN (3)
IPHASJ201550.96+373004.2	SySt	Mira	YSO	SySt	SySt	SySt	AeBe	Be/YSO? (1,2)
IPHASJ202058.52+380949.8	SySt	Mira	YSO	SySt	SySt	SySt	SySt	
IPHASJ202947.93+355926.5	SySt	Mira	YSO	SySt	SySt	ClTTauri	AeBe	YSO (3,4)
IPHASJ204713.69+463517.5	SySt	Mira	YSO	SySt	SySt	SySt	AeBe	
IPHASJ215628.47+571445.5	SySt	Mira	YSO	SySt	SySt	SySt	AeBe	
IPHASJ231735.92+634506.4	SySt	Mira	YSO	SySt	SySt	SySt	AeBe	
IPHASJ203413.39+410157.9	SySt	Mira	YSO	SySt	SySt	ClTTauri	AeBe	
IPHASJ191017.43+065258.1	SySt	Mira	YSO	SySt	SySt	SySt	AeBe	
VPHAS+								
stellar								
VPHASDR2J174455.7-341418.0	SySt	SySt	SySt	SySt	SySt	SySt	SySt	355.39-02.6, known SySt
VPHASDR2J174354.4-330845.3	SySt	SySt	SySt	SySt	SySt	SySt	SySt	
VPHASDR2J175313.8-301805.8	SySt	SySt	SySt	SySt	Mgiant	SySt	SySt	PN Bl L, known SySt
VPHASDR2J175059.8-301247.5	SySt	SySt	SySt	SySt	SySt	SySt	SySt	2MASSJ17505978-3012473, ELS
VPHASDR2J175320.4-295327.4	SySt	SySt	SySt	SySt	SySt	SySt	SySt	
VPHASDR2J175225.9-294557.0	SySt	SySt	SySt	SySt	SySt	SySt	SySt	PN Bl 3-14, known SySt
VPHASDR2J175231.2-291534.8	SySt	SySt	SySt	SySt	SySt	SySt	SySt	000.49-01.45, known SySt
VPHASDR2J175346.2-284826.6	SySt	SySt	SySt	SySt	SySt	WTTauri	SySt	
VPHASDR2J173007.4-312706.8	SySt	SySt	SySt	SySt	SySt	SySt	SySt	
VPHASDR2J173123.2-300844.3	PN	SySt	SySt	SySt	SySt	WTTauri	SySt	357.32+01.97, known SySt

Continued on next page

Table C1 – continued from previous page

Name	(a)	(b)	(c)	(d)	(e)	f	(g)	Comments
VPHASDR2J173155.9-301915.6	SySt	SySt	SySt	SySt	SySt	SySt	SySt	
VPHASDR2J173435.5-294822.2	SySt	SySt	SySt	SySt	SySt	SySt	SySt	357.98+01.57, known SySt
VPHASDR2J173416.8-292912.0	SySt	SySt	SySt	SySt	SySt	SySt	SySt	PN Th 3-31, known SySt
VPHASDR2J173227.9-290509.1	SySt	SySt	SySt	SySt	SySt	SySt	SySt	PN Th 3-29, known SySt
VPHASDR2J171755.8-300142.6	SySt	SySt	SySt	SySt	SySt	SySt	SySt	PN Sa 3-43, known SySt
VPHASDR2J172102.5-292252.8	SySt	SySt	SySt	SySt	SySt	SySt	SySt	PN Th 3-7, known SySt
VPHASDR2J172830.6-292124.5	SySt	SySt	SySt	SySt	SySt	SySt	SySt	ELS
VPHASDR2J172731.6-290256.4	SySt	SySt	SySt	SySt	SySt	SySt	SySt	PN Th 3-17, known SySt
VPHASDR2J173558.5-284954.1	SySt	SySt	SySt	SySt	SySt	SySt	SySt	NSV 22840, known SySt
VPHASDR2J174513.7-265242.9	SySt	SySt	SySt	SySt	SySt	SySt	SySt	Carbon star
VPHASDR2J174055.7-274748.4	SySt	SySt	SySt	SySt	SySt	SySt	SySt	Variable star
VPHASDR2J173343.4-280721.2	SySt	SySt	SySt	SySt	SySt	SySt	SySt	PN Th 3-30, known SySt
VPHASDR2J175648.7-285837.0	SySt	SySt	SySt	SySt	SySt	SySt	SySt	OGLE BLG-LPV 134361, SR-PS
VPHASDR2J175704.2-285034.8	SySt	SySt	SySt	SySt	SySt	SySt	SySt	
VPHASDR2J175645.2-285154.4	SySt	SySt	SySt	SySt	Mgiant	WTTauri	SySt	
VPHASDR2J175828.0-283342.0	SySt	SySt	SySt	SySt	SySt	SySt	SySt	PN H 2-34, known SySt
VPHASDR2J175732.5-271825.3	SySt	SySt	SySt	SySt	SySt	SySt	SySt	PHR 1757-2718, known SySt
VPHASDR2J180913.0-253521.9	SySt	SySt	SySt	SySt	Mgiant	SySt	SySt	
VPHASDR2J180924.9-253834.8	SySt	SySt	SySt	SySt	SySt	WTTauri	SySt	
VPHASDR2J180920.2-253738.5	SySt	SySt	SySt	SySt	SySt	SySt	SySt	
VPHASDR2J180923.8-253158.5	SySt	SySt	SySt	SySt	SySt	SySt	SySt	
VPHASDR2J180910.5-253003.1	SySt	SySt	SySt	SySt	Mgiant	SySt	SySt	
VPHASDR2J180910.6-253023.6	SySt	SySt	SySt	SySt	SySt	WTTauri	SySt	
VPHASDR2J180912.0-253053.3	SySt	SySt	SySt	SySt	Mgiant	SySt	SySt	
VPHASDR2J180914.2-253827.1	SySt	SySt	SySt	SySt	Mgiant	SySt	SySt	
VPHASDR2J180913.6-253106.5	SySt	SySt	SySt	SySt	Mgiant	SySt	SySt	
VPHASDR2J180915.7-252939.1	SySt	SySt	SySt	SySt	Mgiant	SySt	SySt	
VPHASDR2J180910.0-253622.8	SySt	SySt	SySt	SySt	SySt	SySt	SySt	
VPHASDR2J181154.5-243536.2	SySt	SySt	SySt	SySt	SySt	SySt	SySt	2MASSJ18115453-2435360, ELS
VPHASDR2J181333.6-245225.0	SySt	SySt	SySt	SySt	SySt	SySt	SySt	[KW2003] 98, ELS
VPHASDR2J180934.5-245744.2	SySt	SySt	SySt	SySt	SySt	SySt	SySt	
VPHASDR2J181123.2-241430.0	SySt	SySt	SySt	SySt	SySt	SySt	SySt	2MASSJ18112322-2414299, ELS
VPHASDR2J174512.6-253207.2	SySt	SySt	SySt	SySt	SySt	SySt	SySt	
VPHASDR2J174356.1-250625.6	SySt	SySt	SySt	SySt	SySt	SySt	SySt	
VPHASDR2J175527.9-222339.6	SySt	SySt	SySt	SySt	SySt	SySt	SySt	
VPHASDR2J181705.6-153203.8	SySt	SySt	SySt	SySt	SySt	SySt	SySt	
VPHASDR2J185821.0-071139.5	SySt	SySt	SySt	SySt	Kgiant	WTTauri	SySt	
VPHASDR2J184835.7-064110.4	SySt	SySt	SySt	SySt	SySt	SySt	SySt	AS 323, known SySt
VPHASDR2J191333.7+021813.1	SySt	SySt	SySt	SySt	SySt	SySt	SySt	V352 Aql, known SySt
VPHASDR2J141301.4-653320.1	SySt	SySt	SySt	SySt	SySt	SySt	SySt	WRAY 15-1180, ELS
VPHASDR2J160910.9-530245.4	SySt	SySt	SySt	SySt	SySt	SySt	SySt	
VPHASDR2J165421.0-404248.0	SySt	SySt	SySt	SySt	SySt	WTTauri	SySt	
dusty								
VPHASDR2J175016.7-305734.6	SySt	Mira	YSO	SySt	SySt	SySt	SySt	WRAY 16-312, Known SySt
VPHASDR2J175153.5-293053.5	SySt	Mira	YSO	SySt	SySt	SySt	AeBe	variable star
VPHASDR2J173030.0-304937.2	SySt	Mira	YSO	SySt	SySt	SySt	AeBe	
VPHASDR2J173204.8-302854.6	SySt	Mira	YSO	SySt	SySt	ClTTauri	AeBe	
VPHASDR2J173522.2-294519.8	SySt	Mira	YSO	SySt	SySt	SySt	AeBe	Hen 2-251 Known SySt
VPHASDR2J175821.9-281452.2	SySt	Mira	YSO	SySt	SySt	SySt	SySt	PN H 1-45 Known SySt
VPHASDR2J180149.5-195828.4	SySt	Mira	YSO	SySt	SySt	SySt	SySt	
VPHASDR2J180803.5-203454.0	SySt	Mira	YSO	SySt	SySt	ClTTauri	AeBe	posible YSO
VPHASDR2J182047.1-173627.3	SySt	Mira	YSO	SySt	SySt	SySt	SySt	
VPHASDR2J182503.1-143031.5	SySt	Mira	YSO	SySt	SySt	ClTTauri	SySt	
VPHASDR2J183013.2-135356.7	SySt	Mira	YSO	SySt	SySt	SySt	AeBe	Known PN
VPHASDR2J182831.5-122059.5	SySt	Mira	YSO	SySt	SySt	SySt	SySt	
VPHASDR2J182606.0-122839.3	SySt	Mira	YSO	SySt	SySt	ClTTauri	SySt	
VPHASDR2J184024.2-084346.3	SySt	Mira	YSO	SySt	SySt	SySt	SySt	PN K 3-9 Known SySt
VPHASDR2J183910.8-085644.4	SySt	Mira	YSO	SySt	SySt	ClTTauri	AeBe	
VPHASDR2J183044.6-100757.4	SySt	Mira	YSO	SySt	SySt	SySt	SySt	

Continued on next page

Table C1 – continued from previous page

Name	(a)	(b)	(c)	(d)	(e)	f	(g)	Comments
VPHASDR2J184303.6-050026.4	SySt	Mira	YSO	SySt	SySt	SySt	SySt	AGB star
VPHASDR2J184532.1-005029.4	SySt	Mira	YSO	SySt	SySt	SySt	AeBe	
VPHASDR2J184229.2-002144.1	SySt	Mira	YSO	SySt	SySt	SySt	AeBe	
VPHASDR2J101521.0-570706.0	SySt	Mira	YSO	SySt	SySt	SySt	AeBe	
VPHASDR2J124845.2-634948.6	SySt	Mira	YSO	SySt	SySt	SySt	SySt	
VPHASDR2J133405.8-623745.7	SySt	Mira	YSO	SySt	SySt	SySt	AeBe	AGB star
VPHASDR2J133509.6-614305.8	SySt	Mira	YSO	SySt	SySt	SySt	AeBe	ELS
VPHASDR2J154125.6-565953.2	SySt	Mira	YSO	SySt	SySt	ClTTauri	AeBe	
VPHASDR2J152144.3-572220.6	SySt	Mira	YSO	SySt	SySt	SySt	AeBe	
VPHASDR2J160631.4-525616.4	SySt	Mira	YSO	SySt	SySt	SySt	SySt	
VPHASDR2J164646.3-454758.3	SySt	Mira	YSO	SySt	SySt	SySt	SySt	WR star
VPHASDR2J162446.2-485536.4	SySt	Mira	YSO	SySt	SySt	SySt	SySt	
VPHASDR2J162457.4-484340.2	SySt	Mira	YSO	SySt	SySt	SySt	AeBe	ELS
VPHASDR2J164300.8-452701.3	SySt	Mira	YSO	SySt	SySt	SySt	SySt	
VPHASDR2J165346.7-434931.0	SySt	Mira	YSO	SySt	SySt	SySt	AeBe	
VPHASDR2J171225.1-412555.4	SySt	Mira	YSO	SySt	SySt	SySt	AeBe	
VPHASDR2J171455.1-393311.7	SySt	Mira	YSO	SySt	SySt	SySt	AeBe	SySt candidate
VPHASDR2J171527.4-390209.2	SySt	Mira	YSO	SySt	SySt	SySt	AeBe	
VPHASDR2J171513.5-364633.2	SySt	Mira	YSO	SySt	SySt	ClTTauri	SySt	
VPHASDR2J171445.0-361838.4	SySt	Mira	YSO	SySt	SySt	ClTTauri	Syst	ELS
VPHASDR2J120916.3-633202.7	SySt	Mira	YSO	SySt	SySt	SySt	SySt	

The classification of some sources as emission line stars (ELS), semi regular pulsating star (SR-PS), asymptotic giant branch stars (AGB), Wolf-Rayet stars (WR), planetary nebula (PN) or known/candidate symbiotic stars (SySt) is based on the SIMBAD catalogue, Kohoutek & Wehmeyer (2003) or Paper I.
(1) Rodríguez-Flores et al. 2014, (2) Corradi et al. 2010, (3) Viironen et al. (2009b), (4) Krause et al. (2003)

Table C2: NNew very likely symbiotic stars found in Paper I and the IPHAS and VPHAS+ surveys. A further classification of the candidates based on the LDA/KNN analysis is given in columns 2 to 8: (a) SySts/PNe/Be, (b) SySts/CV/Mira, (c) SySts/CV/YSO, (d) SySts/WR/post-AGB, (e) SySts/K-giants/M-giants, (f) SySts/WTT/ClTT, (g) SySts/Be/AeBe.

Name	(a)	(b)	(c)	(d)	(e)	(f)	(g)	Comments
Candidates – Paper I								
stellar								
Hen 3-653	SySt (1.00)	SySt (0.71)	SySt (1.00)	SySt (1.00)	SySt (0.85)	SySt (1.00)	SySt (1.00)	
Hen 4-134	SySt (1.00)	Mira (1.00)	SySt (1.00)	SySt (1.00)	Kgiant (0.85)	SySt (1.00)	SySt (0.86)	
Hen 4-137	SySt (1.00)	SySt (0.71)	SySt (1.00)	SySt (1.00)	Mgiant (1.00)	SySt (1.00)	SySt (1.00)	
V748 Cen	SySt (1.00)	Mira (0.71)	SySt (0.86)	SySt (1.00)	Mgiant (0.85)	WTTauri (0.57)	SySt (0.86)	
WRAY 16-294	SySt (1.00)	SySt (0.86)	SySt (0.86)	SySt (0.57)	Mgiant (0.43)	SySt (1.00)	SySt (0.86)	
001.97+02.41	SySt (1.00)	SySt (1.00)	SySt (0.86)	SySt (1.00)	SySt (1.00)	SySt (0.71)	SySt (1.00)	
001.33+01.07	SySt (1.00)	SySt (1.00)	SySt (1.00)	SySt (1.00)	SySt (1.00)	SySt (1.00)	SySt (1.00)	
001.71+01.14	SySt (1.00)	SySt (1.00)	SySt (1.00)	SySt (0.86)	SySt (1.00)	SySt (1.00)	SySt (1.00)	
DASCH J075731.1+201735	SySt (1.00)	Mira (0.71)	SySt (1.00)	SySt (1.00)	Mgiant (0.85)	SySt (1.00)	SySt (0.86)	
ASAS J174600-2321.3	SySt (1.00)	SySt (1.00)	SySt (1.00)	SySt (0.86)	SySt (1.00)	SySt (0.71)	SySt (1.00)	
dusty								
2MASSJ17145509-393311712	SySt (1.00)	SySt (0.57)	SySt (0.57)	SySt (1.00)	SySt (1.00)	SySt (1.00)	SySt (0.86)	
357.12+01.66	SySt (0.85)	SySt (0.71)	SySt (0.86)	SySt (1.00)	SySt (1.00)	SySt (1.00)	SySt (0.86)	
AS 288	SySt (0.85)	Mira (0.57)	YSO (0.86)	SySt (0.57)	SySt (1.00)	SySt (1.00)	SySt (0.86)	
IPHAS								
stellar								
IPHASJ182906.08-003457.2	SySt (1.00)	SySt (1.00)	SySt (0.86)	SySt (1.00)	SySt (1.00)	SySt (1.00)	SySt (1.00)	known SySt
IPHASJ183501.83+014656.0	SySt (1.00)	SySt (1.00)	SySt (1.00)	SySt (0.86)	SySt (1.00)	SySt (1.00)	SySt (1.00)	known SySt
DQ Ser	SySt (1.00)	SySt (0.86)	SySt (1.00)	SySt (1.00)	SySt (0.85)	SySt (1.00)	SySt (1.00)	known SySt
IPHASJ184446.08+060703.5	SySt (1.00)	SySt (1.00)	SySt (1.00)	SySt (1.00)	SySt (0.57)	SySt (1.00)	SySt (1.00)	known SySt
IPHASJ184733.03+032554.3	SySt (1.00)	SySt (1.00)	SySt (1.00)	SySt (1.00)	SySt (1.00)	SySt (1.00)	SySt (1.00)	known SySt
IPHASJ185039.20+065916.7	SySt (1.00)	SySt (1.00)	YSO (0.71)	SySt (1.00)	SySt (1.00)	SySt (1.00)	SySt (1.00)	
IPHASJ185323.58+084955.0	SySt (1.00)	SySt (1.00)	SySt (1.00)	SySt (1.00)	SySt (1.00)	SySt (1.00)	SySt (1.00)	known SySt
IPHASJ190924.64-010910.2	SySt (1.00)	SySt (1.00)	SySt (0.71)	SySt (0.86)	SySt (0.85)	SySt (0.71)	SySt (1.00)	known SySt
Ap 3-1	SySt (1.00)	SySt (1.00)	SySt (0.71)	SySt (1.00)	Mgiant (0.57)	SySt (1.00)	SySt (1.00)	known SySt
IPHASJ193436.06+163128.9	SySt (1.00)	SySt (1.00)	SySt (1.00)	SySt (0.86)	SySt (1.00)	SySt (0.86)	SySt (1.00)	known SySt
IPHASJ193501.31+135427.5	SySt (1.00)	SySt (1.00)	SySt (0.71)	SySt (1.00)	SySt (1.00)	SySt (1.00)	SySt (1.00)	known SySt
IPHASJ194120.77+245612.9	SySt (1.00)	SySt (1.00)	SySt (0.71)	SySt (1.00)	SySt (1.00)	SySt (1.00)	SySt (1.00)	
dusty								
IPHASJ192257.72+113854.8	SySt (0.57)	SySt (1.00)	YSO (0.85)	SySt (0.57)	SySt (1.00)	SySt (1.00)	SySt (1.00)	
IPHASJ194907.23+211742.0	SySt (0.71)	SySt (0.86)	YSO (1.00)	WR (0.57)	SySt (1.00)	SySt (0.86)	SySt (1.00)	young PN (3)
IPHASJ195712.42+301316.1	SySt (0.71)	Mira (0.86)	YSO (1.00)	WR (1.00)	SySt (0.86)	ClTTauri (0.75)	AeBE (0.71)	young PN (3)
IPHASJ201550.96+373004.2	SySt (0.71)	Mira (0.86)	YSO (1.00)	WR (0.86)	SySt (1.00)	SySt (0.85)	SySt (0.71)	Be/YSO? (1,2)
IPHASJ202058.52+380949.8	SySt (0.86)	Mira (0.86)	YSO (1.00)	WR (1.00)	SySt (0.86)	SySt (1.00)	AeBe (0.43)	
IPHASJ202947.93+355926.5	SySt (0.71)	Mira (0.86)	YSO (0.86)	SySt (0.71)	SySt (1.00)	SySt (0.63)	SySt (0.57)	YSO (3,4)
IPHASJ204713.69+463517.5	SySt (0.57)	Mira (0.71)	YSO (0.71)	WR (0.57)	SySt (0.85)	ClTTauri (0.86)	AeBe (0.71)	
IPHASJ215628.47+571445.5	SySt (0.43)	SySt (0.71)	YSO (1.00)	WR (1.00)	SySt (1.00)	ClTTauri (0.71)	Be (0.57)	
IPHASJ231735.92+634506.4	SySt (0.71)	Mira (1.00)	YSO (1.00)	WR (0.57)	SySt (1.00)	SySt (0.86)	SySt (0.57)	
IPHASJ203413.39+410157.9	SySt (0.86)	SySt (1.00)	YSO (0.86)	SySt (1.00)	SySt (1.00)	SySt (1.00)	SySt (1.00)	
IPHASJ191017.43+065258.1	SySt (0.86)	Mira (0.71)	YSO (0.86)	SySt (0.57)	SySt (1.00)	SySt (0.57)	SySt (0.57)	
VPHAS+								
stellar								
VPHASDR2J174455.7-341418.0	SySt (1.00)	SySt (1.00)	SySt (1.00)	SySt (1.00)	SySt (1.00)	SySt (1.00)	SySt (1.00)	355.39-02.6, known SySt
VPHASDR2J174354.4-330845.3	SySt (1.00)	SySt (1.00)	SySt (0.71)	SySt (1.00)	SySt (1.00)	SySt (1.00)	SySt (1.00)	
VPHASDR2J175313.8-301805.8	SySt (1.00)	SySt (1.00)	SySt (1.00)	SySt (0.86)	SySt (1.00)	SySt (0.57)	SySt (1.00)	PN Bl L, known SySt
VPHASDR2J175059.8-301247.5	SySt (1.00)	SySt (1.00)	SySt (0.86)	SySt (1.00)	SySt (1.00)	SySt (1.00)	SySt (1.00)	2MASSJ17505978-3012473, ELS
VPHASDR2J175320.4-295327.4	SySt (1.00)	SySt (1.00)	SySt (1.00)	SySt (1.00)	SySt (1.00)	SySt (1.00)	SySt (1.00)	
VPHASDR2J175225.9-294557.0	SySt (1.00)	SySt (1.00)	SySt (1.00)	SySt (1.00)	SySt (1.00)	SySt (1.00)	SySt (1.00)	PN Bl 3-14, known SySt
VPHASDR2J175231.2-291534.8	SySt (1.00)	SySt (0.86)	SySt (1.00)	SySt (1.00)	SySt (1.00)	SySt (1.00)	SySt (1.00)	000.49-01.45, known SySt
VPHASDR2J175346.2-284826.6	SySt (1.00)	SySt (1.00)	SySt (1.00)	SySt (1.00)	SySt (1.00)	SySt (0.86)	SySt (1.00)	
VPHASDR2J173007.4-312706.8	SySt (1.00)	SySt (1.00)	SySt (0.86)	SySt (1.00)	SySt (1.00)	SySt (1.00)	SySt (1.00)	

Continued on next page

Table C2 – continued from previous page

Name	(a)	(b)	(c)	(d)	(e)	f	(g)	Comments
VPHASDR2J173123.2-300844.3	SySt (0.85)	SySt (1.00)	SySt (0.85)	SySt (1.00)	SySt (1.00)	SySt (0.57)	SySt (1.00)	357.32+01.97, known SySt
VPHASDR2J173155.9-301915.6	SySt (1.00)	SySt (1.00)	SySt (1.00)	SySt (1.00)	SySt (1.00)	SySt (1.00)	SySt (1.00)	
VPHASDR2J173435.5-294822.2	SySt (1.00)	SySt (1.00)	SySt (0.86)	SySt (1.00)	SySt (1.00)	SySt (1.00)	SySt (1.00)	357.98+01.57, known SySt
VPHASDR2J173416.8-292912.0	SySt (1.00)	SySt (1.00)	SySt (0.86)	SySt (0.86)	SySt (1.00)	SySt (0.71)	SySt (1.00)	PN Th 3-31, known SySt
VPHASDR2J173227.9-290509.1	SySt (1.00)	SySt (0.86)	SySt (1.00)	SySt (1.00)	SySt (1.00)	SySt (1.00)	SySt (1.00)	PN Th 3-29, known SySt
VPHASDR2J171755.8-300142.6	SySt (1.00)	SySt (1.00)	SySt (1.00)	SySt (1.00)	SySt (1.00)	SySt (1.00)	SySt (0.86)	PN Sa 3-43, known SySt
VPHASDR2J172102.5-292252.8	SySt (1.00)	SySt (1.00)	SySt (1.00)	SySt (1.00)	SySt (1.00)	SySt (1.00)	SySt (0.86)	PN Th 3-7, known SySt
VPHASDR2J172830.6-292124.5	SySt (1.00)	SySt (0.86)	SySt (1.00)	SySt (1.00)	SySt (0.71)	SySt (1.00)	SySt (1.00)	ELS
VPHASDR2J172731.6-290256.4	SySt (1.00)	SySt (1.00)	SySt (1.00)	SySt (0.86)	SySt (1.00)	SySt (1.00)	SySt (1.00)	PN Th 3-17, known SySt
VPHASDR2J173558.5-284954.1	SySt (1.00)	SySt (1.00)	SySt (1.00)	SySt (1.00)	SySt (1.00)	SySt (0.71)	SySt (1.00)	NSV 22840, known SySt
VPHASDR2J174513.7-265242.9	SySt (1.00)	SySt (1.00)	SySt (1.00)	SySt (1.00)	SySt (1.00)	SySt (1.00)	SySt (1.00)	Carbon star
VPHASDR2J174055.7-274748.4	SySt (1.00)	SySt (1.00)	SySt (1.00)	SySt (1.00)	SySt (1.00)	SySt (1.00)	SySt (1.00)	Variable star
VPHASDR2J173343.4-280721.2	SySt (1.00)	SySt (1.00)	SySt (1.00)	SySt (1.00)	SySt (1.00)	SySt (1.00)	SySt (1.00)	PN Th 3-30, known SySt
VPHASDR2J175648.7-285837.0	SySt (1.00)	SySt (1.00)	SySt (1.00)	SySt (1.00)	SySt (1.00)	SySt (0.86)	SySt (1.00)	OGLE BLG-LPV 134361, SR-PS
VPHASDR2J175704.2-285034.8	SySt (1.00)	SySt (1.00)	SySt (1.00)	SySt (1.00)	SySt (1.00)	SySt (1.00)	SySt (1.00)	
VPHASDR2J175645.2-285154.4	SySt (1.00)	SySt (1.00)	YSO (0.57)	SySt (1.00)	SySt (1.00)	WTTauri (1.00)	SySt (1.00)	
VPHASDR2J175828.0-283342.0	SySt (1.00)	SySt (1.00)	SySt (1.00)	SySt (1.00)	SySt (1.00)	SySt (1.00)	SySt (1.00)	PN H 2-34, known SySt
VPHASDR2J175732.5-271825.3	SySt (1.00)	SySt (1.00)	SySt (1.00)	SySt (1.00)	SySt (1.00)	SySt (1.00)	SySt (1.00)	PHR 1757-2718, known SySt
VPHASDR2J180913.0-253521.9	SySt (1.00)	SySt (1.00)	SySt (1.00)	SySt (1.00)	SySt (1.00)	SySt (0.71)	SySt (1.00)	
VPHASDR2J180924.9-253834.8	SySt (1.00)	SySt (1.00)	SySt (0.71)	SySt (1.00)	SySt (1.00)	SySt (0.57)	SySt (1.00)	
VPHASDR2J180920.2-253738.5	SySt (1.00)	SySt (1.00)	SySt (1.00)	SySt (1.00)	SySt (1.00)	SySt (0.71)	SySt (1.00)	
VPHASDR2J180923.8-253158.5	SySt (1.00)	SySt (1.00)	SySt (1.00)	SySt (1.00)	SySt (1.00)	SySt (0.71)	SySt (1.00)	
VPHASDR2J180910.5-253003.1	SySt (1.00)	SySt (1.00)	CV (0.57)	SySt (1.00)	SySt (1.00)	WTTauri (0.86)	SySt (0.86)	
VPHASDR2J180910.6-253023.6	SySt (0.86)	SySt (1.00)	YSO (0.57)	SySt (1.00)	SySt (1.00)	WTTauri (1.00)	SySt (1.00)	
VPHASDR2J180912.0-253053.3	SySt (1.00)	SySt (1.00)	SySt (0.86)	SySt (1.00)	SySt (1.00)	SySt (1.00)	SySt (1.00)	
VPHASDR2J180914.2-253827.1	SySt (1.00)	SySt (1.00)	SySt (1.00)	SySt (1.00)	SySt (1.00)	SySt (0.85)	SySt (1.00)	
VPHASDR2J180913.6-253106.5	SySt (1.00)	SySt (1.00)	SySt (1.00)	SySt (1.00)	SySt (0.86)	SySt (1.00)	SySt (0.86)	
VPHASDR2J180915.7-252939.1	SySt (1.00)	SySt (1.00)	SySt (0.86)	SySt (1.00)	SySt (1.00)	SySt (0.71)	SySt (1.00)	
VPHASDR2J180910.0-253622.8	SySt (1.00)	SySt (1.00)	SySt (0.57)	SySt (1.00)	SySt (1.00)	WTTauri (1.00)	SySt (0.86)	
VPHASDR2J181154.5-243536.2	SySt (1.00)	SySt (1.00)	SySt (0.71)	SySt (1.00)	SySt (1.00)	SySt (1.00)	SySt (1.00)	2MASSJ18115453-2435360, ELS
VPHASDR2J181333.6-245225.0	SySt (1.00)	SySt (1.00)	SySt (0.86)	SySt (1.00)	SySt (1.00)	SySt (0.57)	SySt (1.00)	[KW2003] 98, ELS
VPHASDR2J180934.5-245744.2	SySt (1.00)	SySt (1.00)	SySt (1.00)	SySt (1.00)	SySt (1.00)	SySt (1.00)	SySt (1.00)	
VPHASDR2J181123.2-241430.0	SySt (1.00)	SySt (1.00)	SySt (1.00)	SySt (1.00)	SySt (1.00)	SySt (1.00)	SySt (1.00)	2MASSJ18112322-2414299, ELS
VPHASDR2J174512.6-253207.2	SySt (1.00)	SySt (1.00)	SySt (0.86)	SySt (1.00)	SySt (1.00)	SySt (0.86)	SySt (1.00)	
VPHASDR2J174356.1-250625.6	SySt (1.00)	SySt (1.00)	SySt (0.86)	SySt (1.00)	SySt (1.00)	SySt (1.00)	SySt (1.00)	
VPHASDR2J175527.9-222339.6	SySt (1.00)	SySt (1.00)	SySt (1.00)	SySt (1.00)	SySt (1.00)	SySt (1.00)	SySt (1.00)	
VPHASDR2J181705.6-153203.8	SySt (1.00)	SySt (1.00)	SySt (1.00)	SySt (1.00)	SySt (1.00)	SySt (1.00)	SySt (1.00)	
VPHASDR2J185821.0-071139.5	SySt (1.00)	SySt (0.86)	SySt (0.43)	SySt (1.00)	SySt (1.00)	WTTauri (0.86)	SySt (1.00)	
VPHASDR2J184835.7-064110.4	SySt (1.00)	SySt (0.86)	SySt (1.00)	SySt (1.00)	Mgiant (0.42)	SySt (1.00)	SySt (1.00)	AS 323, known SySt
VPHASDR2J191333.7+021813.1	SySt (1.00)	SySt (1.00)	SySt (1.00)	SySt (1.00)	Kgiant (0.71)	SySt (1.00)	SySt (1.00)	V352 Aql, known SySt
VPHASDR2J141301.4-653320.1	SySt (1.00)	SySt (1.00)	SySt (1.00)	SySt (1.00)	SySt (0.71)	SySt (1.00)	SySt (1.00)	WRAY 15-1180, ELS
VPHASDR2J160910.9-530245.4	SySt (1.00)	SySt (1.00)	SySt (1.00)	SySt (1.00)	SySt (1.00)	SySt (1.00)	SySt (1.00)	
VPHASDR2J165421.0-404248.0	SySt (0.71)	SySt (1.00)	CV (0.57)	SySt (1.00)	SySt (1.00)	WTTauri (0.86)	SySt (1.00)	
dusty								
VPHASDR2J175016.7-305734.6	SySt (1.00)	SySt (1.00)	YSO (0.86)	SySt (1.00)	SySt (1.00)	SySt (1.00)	SySt (1.00)	WRAY 16-312, Known SySt
VPHASDR2J175153.6-293053.5	SySt (0.86)	SySt (0.75)	SySt (0.57)	SySt (0.86)	SySt (1.00)	SySt (0.86)	SySt (0.71)	variable star
VPHASDR2J173030.0-304937.2	SySt (0.86)	Mira (0.57)	SySt (0.57)	SySt (0.86)	SySt (1.00)	SySt (1.00)	SySt (1.00)	
VPHASDR2J173204.8-302854.6	SySt (0.86)	SySt (0.71)	SySt (0.85)	SySt (1.00)	SySt (1.00)	SySt (1.00)	SySt (0.86)	
VPHASDR2J173522.2-294519.8	SySt (0.86)	SySt (1.00)	SySt (0.71)	SySt (0.57)	SySt (1.00)	SySt (1.00)	SySt (0.57)	Hen 2-251 Known SySt
VPHASDR2J175821.9-281452.2	SySt (1.00)	SySt (0.86)	SySt (0.86)	SySt (1.00)	SySt (1.00)	SySt (1.00)	SySt (1.00)	PN H 1-45 Known SySt
VPHASDR2J180149.5-195828.4	SySt (0.86)	SySt (0.86)	YSO (0.86)	SySt (0.86)	SySt (1.00)	SySt (0.86)	SySt (0.86)	
VPHASDR2J180803.5-203454.0	SySt (0.57)	Mira (0.86)	YSO (1.00)	SySt (0.71)	SySt (1.00)	SySt (1.00)	SySt (0.86)	posible YSO
VPHASDR2J182047.1-173627.3	SySt (1.00)	SySt (1.00)	SySt (1.00)	SySt (1.00)	SySt (1.00)	SySt (1.00)	SySt (0.86)	
VPHASDR2J182503.1-143031.5	SySt (0.86)	SySt (0.71)	SySt (0.86)	SySt (1.00)	SySt (1.00)	SySt (1.00)	SySt (1.00)	
VPHASDR2J183013.2-135356.7	SySt (1.00)	SySt (1.00)	SySt (1.00)	SySt (1.00)	SySt (1.00)	SySt (1.00)	SySt (0.71)	Known PN
VPHASDR2J182831.5-122059.5	SySt (1.00)	Mira (0.86)	YSO (0.57)	SySt (1.00)	SySt (1.00)	SySt (1.00)	SySt (0.71)	
VPHASDR2J182606.0-122839.3	SySt (0.86)	SySt (0.71)	SySt (1.00)	SySt (0.86)	SySt (1.00)	SySt (1.00)	SySt (1.00)	
VPHASDR2J184024.2-084346.3	SySt (1.00)	Mira (0.86)	YSO (0.86)	SySt (1.00)	SySt (1.00)	ClTTauri (0.86)	SySt (0.86)	PN K 3-9 Known SySt
VPHASDR2J183910.8-085644.4	SySt (0.86)	Mira (0.57)	YSO (1.00)	WR (0.86)	SySt (1.00)	SySt (1.00)	SySt (0.57)	

Continued on next page

Table C2 – continued from previous page

Name	(a)	(b)	(c)	(d)	(e)	f	(g)	Comments
VPHASDR2J183044.6-100757.4	SySt (0.86)	SySt (0.57)	SySt (1.00)	SySt (0.57)	SySt (1.00)	SySt (1.00)	SySt (0.86)	
VPHASDR2J184303.6-050026.4	SySt (0.71)	Mira (0.86)	YSO (1.00)	SySt (1.00)	SySt (1.00)	SySt (0.86)	SySt (0.71)	AGB star
VPHASDR2J184532.1-005029.4	SySt (1.00)	Mira (0.71)	YSO (0.86)	SySt (1.00)	SySt (1.00)	SySt (1.00)	SySt (0.86)	
VPHASDR2J184229.2-002144.1	SySt (1.00)	SySt (0.71)	YSO (1.00)	SySt (1.00)	SySt (1.00)	SySt (1.00)	SySt (1.00)	
VPHASDR2J101521.0-570706.0	SySt (0.71)	Mira (0.86)	YSO (1.00)	WR (0.86)	SySt (0.86)	SySt (0.71)	AeBe (0.86)	
VPHASDR2J124845.2-634948.6	SySt (1.00)	Mira (1.00)	YSO (0.71)	WR (0.71)	SySt (1.00)	SySt (1.00)	AeBe (0.57)	
VPHASDR2J133405.8-623745.7	SySt (0.71)	Mira (0.86)	YSO (0.86)	SySt (0.71)	SySt (1.00)	ClTTauri (0.86)	AeBe (0.86)	AGB star
VPHASDR2J133509.6-614305.8	SySt (0.43)	Mira (0.71)	YSO (0.86)	WR (1.00)	SySt (1.00)	ClTTauri (0.86)	AeBe (0.57)	ELS
VPHASDR2J154125.6-565953.2	SySt (0.86)	SySt (0.57)	YSO (1.00)	SySt (1.00)	SySt (1.00)	SySt (1.00)	SySt (1.00)	
VPHASDR2J152144.3-572220.6	SySt (0.86)	Mira (0.57)	SySt (0.57)	SySt (0.86)	SySt (1.00)	SySt (1.00)	SySt (0.71)	
VPHASDR2J160631.4-525616.4	SySt (0.71)	Mira (0.86)	YSO (0.86)	WR (0.86)	SySt (1.00)	SySt (1.00)	AeBe (0.71)	
VPHASDR2J164646.3-454758.2	SySt (1.00)	SySt (0.86)	SySt (1.00)	SySt (1.00)	SySt (1.00)	SySt (1.00)	SySt (1.00)	WR star
VPHASDR2J162446.2-485536.4	SySt (1.00)	Mira (0.71)	YSO (0.71)	SySt (1.00)	SySt (1.00)	SySt (1.00)	AeBe (0.57)	
VPHASDR2J162457.4-484340.2	SySt (1.00)	Mira (1.00)	YSO (0.71)	WR (0.86)	SySt (1.00)	SySt (1.00)	AeBe (0.86)	ELS
VPHASDR2J164300.8-452701.3	SySt (1.00)	SySt (1.00)	SySt (0.86)	SySt (1.00)	SySt (1.00)	SySt (1.00)	SySt (1.00)	
VPHASDR2J165346.7-434931.0	SySt (0.71)	Mira (0.86)	YSO (0.86)	SySt (1.00)	SySt (1.00)	SySt (1.00)	SySt (0.86)	
VPHASDR2J171225.1-412555.4	SySt (0.86)	Mira (0.86)	YSO (0.86)	SySt (1.00)	SySt (1.00)	SySt (0.86)	SySt (0.86)	
VPHASDR2J171455.1-393311.7	SySt (1.00)	SySt (1.00)	YSO (0.57)	SySt (1.00)	SySt (1.00)	SySt (0.86)	SySt (1.00)	SySt candidate
VPHASDR2J171527.4-390209.2	SySt (1.00)	SySt (0.86)	YSO (0.71)	SySt (1.00)	SySt (1.00)	SySt (1.00)	AeBe (1.00)	
VPHASDR2J171513.5-364633.2	SySt (0.86)	SySt (0.71)	YSO (0.86)	SySt (1.00)	SySt (1.00)	SySt (0.86)	SySt (0.71)	
VPHASDR2J171445.0-361838.4	SySt (0.71)	Mira (0.86)	SySt (1.00)	SySt (1.00)	SySt (1.00)	ClTTauri (0.71)	AeBe (1.00)	ELS
VPHASDR2J120916.3-633202.7	SySt (0.86)	SySt (1.00)	YSO (0.86)	SySt (1.00)	SySt (1.00)	SySt (0.71)	SySt (1.00)	

The classification of some sources as emission line stars (ELS), semi regular pulsating star (SR-PS), asymptotic giant branch stars (AGB), Wolf-Rayet stars (WR), planetary nebula (PN) or known/candidate symbiotic stars (SySt) is based on the SIMBAD catalogue, Kohoutek & Wehmeyer (2003) or Paper I.
(1) Rodríguez-Flores et al. 2014, (2) Corradi et al. 2010, (3) Viironen et al. (2009b), (4) Krause et al. (2003)